

**RELATIONSHIP BETWEEN PRECIPITATION AND  
PRECIPITABLE WATER VAPOR OVER THE  
MARITIME CONTINENT**

A thesis presented

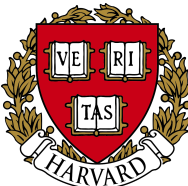
by

Ellen Trim Robo

to

The Department of Earth and Planetary Sciences  
in partial fulfillment of the requirements  
for a degree with honors  
of Bachelor of Arts

April 2016  
Harvard College



## Abstract

Many questions about the Madden Julian Oscillation (MJO) are still unanswered. One among them is why, when it passes over the Maritime Continent, the deep convection associated with the MJO weakens. One theory as to why this happens is a strong diurnal cycle associated with the high percentage of land mass in the Maritime Continent provides a high frequency forcing that disrupts the otherwise low frequency MJO.

In this study, to better understand whether the diurnal cycle is the cause of the convection weakening, the relationship between precipitation and precipitable water vapor is investigated for observations taken over the ocean and over land to see whether they differ. Three different temporal resolutions of precipitation are used to better understand how precipitation changes over the course of a day and as more time is included around a precipitable water vapor observation. The diurnal cycles of precipitation and precipitable water vapor are further investigated as well.

This study finds that the relationship between precipitation and precipitable water vapor differs significantly and statistically over land and ocean. Furthermore, the difference in the relationship is a function of the distance the point of land is from a coast. Land far from a coast experiences cutoff in precipitation for high value of precipitable water vapor. Findings related to the changes seen in the relationship of precipitation and precipitable water vapor as the temporal resolution is changed support a strong diurnal forcing over the land that may be causing the weakening of the MJO as it passes over the Maritime Continent.

# Table of Contents

<b>ABSTRACT .....</b>	<b>II</b>
<b>LIST OF FIGURES .....</b>	<b>V</b>
<b>LIST OF TABLES .....</b>	<b>VI</b>
<b>ACKNOWLEDGEMENTS.....</b>	<b>VII</b>
<b>1. INTRODUCTION .....</b>	<b>1</b>
1.1 OVERVIEW .....	1
1.2 MADDEN JULIAN OSCILLATION .....	2
1.3 THEORIES TO EXPLAIN CONVECTION WEAKENING .....	3
1.4 MARITIME CONTINENT .....	4
1.5 TRMM.....	5
1.6 COSMIC .....	5
1.6.1 <i>How RO Works</i> .....	5
1.6.2 <i>History of Radio Occultation</i> .....	6
1.6.3 <i>COSMIC Data</i> .....	7
1.7 PREVIOUS RESEARCH .....	7
1.8 SUOMINET.....	9
<b>CHAPTER 2: INITIAL ANALYSIS .....</b>	<b>11</b>
2.1 GENERAL METHODS .....	11
2.1.1 <i>PRECIPITABLE WATER VAPOR COLUMN ANALYSIS</i> .....	11
2.1.2 <i>TREATMENT OF THE TRMM DATA</i> .....	12
2.1.3 <i>FINDING THE RELATIONSHIP BETWEEN PRECIPITATION AND PRECIPITABLE WATER</i> .....	13
2.1.4 <i>BOOTSTRAPPING</i> .....	14
2.2 DATA OVERVIEW .....	14
2.3 CLIMATOLOGY OVERVIEW .....	18
2.3.2 <i>Results</i> .....	24
2.4 DIURNAL CYCLE .....	24
2.4.1 <i>PRECIPITABLE WATER VAPOR</i> .....	24
2.4.2 <i>PRECIPITATION</i> .....	27
2.5 RELATIONSHIP BETWEEN PRECIPITATION AND PRECIPITABLE WTER VAPOR.....	28
2.6 STATISTICAL BOUNDS ON RELATIONSHIP.....	32
<b>CHAPTER 3: SUOMINET ANALYSIS .....</b>	<b>35</b>
3.1 METHODS AND RESULTS .....	35
3.2 COMPARING SUOMINET AND COSMIC .....	36
<b>CHAPTER 4: DISTANCE FROM A COAST .....</b>	<b>42</b>
4.1 MOTIVATION .....	42
4.2 METHODS .....	42
4.3 DATA OVERVIEW .....	42
4.4 DUILNAL CYCLES .....	45
4.4.1 <i>PRECIPITABLE WATER VAPOR</i> .....	45
4.4.2 <i>PRECIPITATION</i> .....	46
4.5 RELATIONSHIP BETWEEN PRECIPITATION AND PRECIPITABLE WATER VAPOR BY DISTANCE FROM A COAST .....	47

4.6 STATISTICAL BOUNDS.....	49
<b>CHAPTER 5: AVERAGING COSMIC DATA.....</b>	<b>50</b>
<b>CHAPTER 6: CONCLUSION .....</b>	<b>51</b>
6.1 OVERVIEW OF FINDINGS .....	51
6.2 FURTURE WORK .....	52
<b>REFERENCES .....</b>	<b>53</b>

## List of Figures

1. Map of the Maritime Continent.....	4
2. Diagram of GPS Radio Occultation .....	6
3. Relationship Between Precipitation and Precipitation Water Vapor Over Tropical Oceans and Distribution.....	8
4. Map of SUOMINET Station Locations.....	9
5. Map of COSMIC Observations over the Maritime Continent.....	14
6. Close up of a Section of Map of COSMIC Observations over the Maritime Continent.....	15
7. Histogram of COSMIC Observations .....	16
8. Histogram of Percent of COSMIC Observations.....	17
9. Map of the average COSMIC precipitable water vapor .....	18
10. Map of the average JJA COSMIC precipitable water vapor .....	19
11. Map of the average DJF COSMIC precipitable water vapor .....	20
12. Map of the average TRMM Precipitation .....	21
13. Map of the average JJA TRMM Precipitation .....	22
14. Map of the average DJA TRMM Precipitation .....	23
15. Diurnal cycle of COSMIC Precipitable Water Vapor.....	25
16. Diurnal cycle of each SUOMINET station precipitable water vapor....	26
17. Diurnal cycle of TRMM Precipitation Observations.....	27
18. Plot of the Relationship Between Precipitation and Precipitable Water Vapor.....	29
19. Bootstrapped Plots of Relationship Between Precipitation and Precipitable Water Vapor.....	33
20. Plots of SUOMINET Analysis .....	35
21. Comparison of Close SUOMINET and COMSIC Measurements.....	37
22. Difference Between SUOMINET and COMSMIC by Distance .....	38
23. Histogram of Percent Difference of COSMIC and SUOMINET Measurements .....	39

24. Histogram of Difference in Measurement Between COSMIC and SUOMINET .....	39
25. Histograms of Difference in COSMIC and SUOMINET Measurements by Distance .....	40
26. Map of the Land Divided into Distance From a Coast.....	43
27. Distribution of COSMIC Observations Over Land Divided by Distance From a Coast.....	43
28. Distribution of the Distance from Coast of COSMIC Observations.....	44
29. Diurnal Cycle of COSMIC Observation by Distances From a Coast....	45
30. Diurnal Cycle of TRMM Observations Divided by Distance From a Coast.....	30
31. Daily Mean Precipitation and Precipitable Water Vapor by Distance from a Coast.....	47
32. Bootstrapped Distance from a Coast.....	48

## List of Tables

1. Coordinates for the SUOMINET Stations.....	9
---	---

## Acknowledgements

For this entire process, I have a lot of people to thank. First and foremost, my advisor, Zhiming Kuang. For patiently explaining simple concept and expertly explaining complex ones, for providing guidance through the past year, for perspective, humor, and sanity, for exposing me to research, I am forever grateful for all you have done for me in the past year.

For so many of my friends who have been sounding boards, chocolate supplies, editors, thesaurus, sources of comfort, and expert motivators and cheerleaders. Thank you especially to Natalie and Gillian who made sure I always ate and knew I would finish this thesis. Thank you to Chloe for your overwhelming support— and kitkats. Thank you to Paul for keeping me company through the many evenings I spent coding and writing.

Thank you to the EPS department for providing me with a place to study such wonderful and interesting material and a home these past four years. Thank you to Chenoweth, you never fail to raise my spirits as you answer all the small questions I have. To Esther and Annika, thank you for guiding me through the thesis writing process. To my fellow EPS thesis writers, congratulations and thank you for inspiring me to explore new fields by learning about all of your thesis topics.

# 1. Introduction

## 1.1 OVERVIEW

The Madden Julian Oscillation (MJO) was first identified in 1971 yet, with the forty years of research that have gone into better understanding the phenomena, there are still many unanswered questions. “It is fair to say that the MJO remains an unmet challenge to our understanding of the tropical atmosphere and to our ability to simulate and predict its variability” [Zhang, 2005]. In this thesis, I try to better understand one question surrounding the MJO: why, when it passes over the Maritime Continent, the strong convection associated with the MJO diminishes. I will examine this question by looking at the differences in the relationship between precipitation and precipitable water vapor over the ocean and land in the Maritime Continent.

Predominately using two data sets, COSMIC for precipitable water vapor and TRMM for precipitation, I will collocate precipitable water vapor and precipitation observations to see how the presence of land impacts these two quantities and the relationship between them. I will examine how changes in temporal resolution of precipitation measurements impacts the relationship. I will also examine the diurnal cycles of precipitation and precipitable water vapor. To verify the results from the COSMIC-TRMM analysis, I will use SUOMINET, another project measuring precipitable water vapor. Based on the findings from SUOMINET, I will look at the effect distance from a coast has on the relationship between precipitation and precipitable water vapor.

This thesis finds that the relationship between precipitation and precipitable water vapor is not only dependent on whether it is over ocean or land but it is also dependent on the distance the land is from a coast. While the relationship over the ocean is exponential, consistent with previous research, the relationship over land is exponential until it reaches 55 mm of precipitable water vapor when it flattens out.

## 1.2 MADDEN JULIAN OSCILLATION

The Madden Julian Oscillation (MJO) is characterized by a coupling of climate factors that move eastward across the tropical oceans. The main and most obvious component of the MJO is a 5 m/s eastward propagation of deep convection and precipitation across the equatorial Indian and western/central Pacific oceans. This is known as the “active phase” of the MJO. On the east and west of the active phase are areas of weak deep convection and precipitation. These are known as “inactive phases” [Zhang 2005].

When it was first identified by Madden and Julian in the 1970s, the MJO was referred to as the 40-50 day tropical oscillation [*Madden and Julian 1971*]. Since then, the period of the oscillation changes depending on who is discussing the MJO [*Zhang, 2005; Randall, 2015*]. Despite the lack of consistency on the exact range of the MJO, the time period is intraseasonal. One of the reasons the MJO has been the focus of so much research in the last few decades is the hope, due to its time period, an understanding of the MJO will lead to better predictions of weather patterns and anomalies within the tropics [*Randall, 2015*].

However, the mechanism behind the MJO is currently unknown and general circulation models do not predict it well. Progress has been made in the last few decades to better understand why it is not well predicted in the models [*Zhang, 2005*].

The MJO experiences seasonal variability. It is strongest during austral summer and fall south of the equator, corresponding with the Australian monsoon season. Its second peak is during boreal summer and fall north of the equator, corresponding to the Asian monsoon season [*Zhang, 2005*].

The MJO interacts differently over the Maritime Continent than it does over the rest of its main path in the Indian and western/central Pacific oceans. While there is evidence that components of the MJO

continue over South America [*Randall, 2015*] and the rest of the equator [*Madden and Julian 1994*], the main active phase is not seen in these areas. This makes the Maritime Continent the only portion of the MJO's path obstructed by substantial land masses.

### 1.3 THEORIES TO EXPLAIN CONVECTION WEAKENING

While there are several theories as to why this weakening occurs, it is not well understood and many studies put forth different theories. All of the theories center on various differences between land and ocean: topography, surface evaporation, turbulent fluxes, and heating coefficients [*Zhang, 2005*]. The friction resulting from the topography of the Maritime Continent potentially inhibits circulation in the boundary layer [*Zhang and Hendon, 1996; Wang and Li, 1994*]. Turbulent fluxes are thought to potentially explain the weakening because while they exist over the ocean and may be a source of energy for the MJO, they do not exist over the land [*Zhang and Hendon, 1997*]. Surface evaporation, thought to be very important for the MJO is significantly reduced over land which might explain the weakening [*Zhang, 2005*]. Maloney and Sobel [2004] examined the impact different mixing layers within the ocean would have on the MJO using a general circulation model (GCM). While their GCM could not resolve the islands, when using a shallow mixing layer, their model saw a drop in the amplitude of the MJO similar to what is seen over the Maritime Continent. One possible explanation for why a shallow mixing layer in the ocean might approximate the Maritime Continent is, when the MJO is strongest during austral summer, the Maritime Continent receives a considerable amount of water. This may lead the ground to be saturated to the point that it reacts like a shallow mixed layer.

The theory that currently has the most support is the diurnal cycle due to heating coefficients weakening the MJO over the Maritime Continent. Land has a much smaller heating coefficient than the ocean

which leads to a stronger diurnal cycle. This overriding diurnal cycle potentially competes for moist static energy with the MJO, introducing a high frequency overturning of convection drastically different from the relatively low frequency MJO, diminishing the strength of the MJO's active phase [Salby and Hendon, 1993; Wang and Li, 1994; Zhang and Hendon, 1996].

There are several reasons which I think contribute to the current lack of a concrete understanding of this phenomena. It is a challenging area to study. Resolving the islands in the Maritime Continent is not possible for many general circulation models [Maloney and Sobel, 2004]. The area is not geographically large leading to few measurements for globally collected data sets. I encounter this problem in this thesis. Even with ten years of data, I encounter much noise in some of my plots.

#### 1.4 MARITIME CONTINENT

The area under investigation in this thesis is the Maritime Continent defined as  $15^{\circ}\text{S}$  to  $20^{\circ}\text{N}$  and  $90^{\circ}\text{E}$  to  $150^{\circ}\text{E}$ , as shown in Figure 1. It is an area in the western Pacific Ocean that contains a high percent of islands in the tropics.

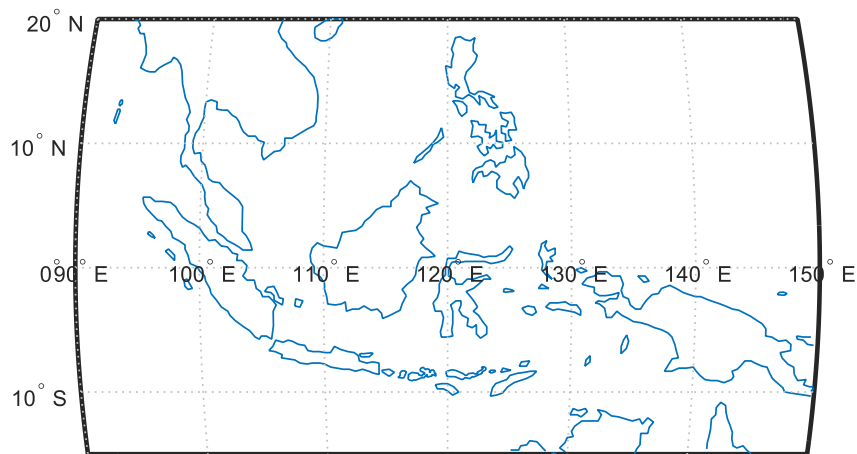


**Figure 1| Map of the Maritime Continent**

## 1.5 TRMM

This studies relies upon data from the Tropical Rainfall Measuring Mission (TRMM), a joint project between NASA and the Japan Aerospace Exploration Agency. TRMM was launched on November 27, 1997 with a mission of better understanding the rainfall in the tropics and how changes in rainfall interact with the rest of the climate [*TRMM Factsheet*]. The radar used by TRMM allows for measurements of precipitation.

The TRMM data product used is 3B42 version 7 with a 3-hour temporal resolution and a 0.25x0.25 degree spatial resolution.

## 1.6 COSMIC

The main source of precipitable water vapor measurements for this thesis is the Constellation Observing System for Meteorology, Ionosphere, and Climate (COSMIC). On April 15, 2006, six COSMIC satellites were launched from Vandenberg Air Force Base in California. COSMIC is a joint program between UCAR and National Space Organization in Taiwan and the first to use GPS radio occultation (RO) at a large scale to gather information about Earth's atmosphere.

### 1.6.1 How RO Works

Most satellites collecting information about the atmosphere send out a wave; it hits the earth, reflects, and returns to the satellite. The time it takes to leave and return is measured and from this time, information about the atmosphere is inferred. Before COSMIC and the widespread use of RO, microwave satellite programs had been used to retrieve measurements of water vapor in the atmosphere, but this was only effective over the ocean. Because of the emission of microwaves off land, using microwaves as the signal to measure water vapor in the atmosphere was impossible [*Bretherton et al, 2004*].

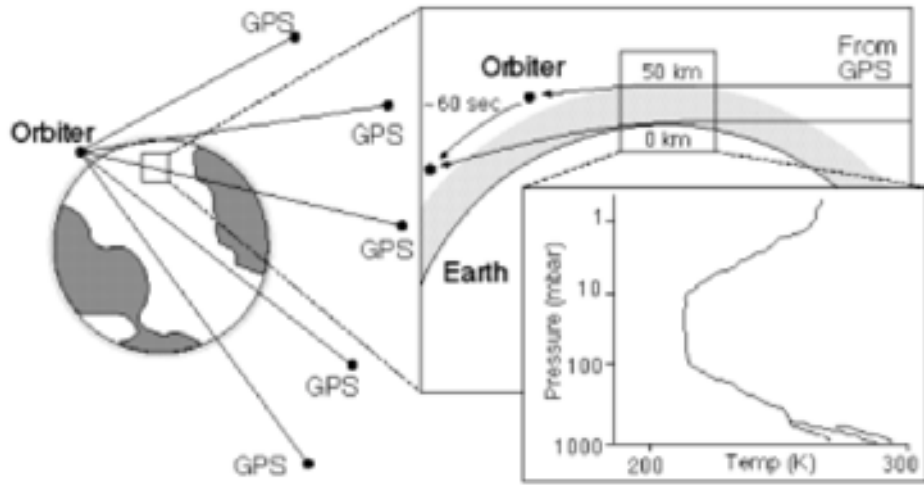


**Figure 2| Diagram of GPS Radio Occultation** (Source: Yunck *et al*, 2000)

RO instead uses two satellites, a GPS satellite and an occultation receiver to look only at the atmosphere and not interact with the Earth's surface. As the signal passes from the GPS to the receiver through the atmosphere, the presence of the atmosphere causes the signal to refract. The amount it refracts by is dependent on the water vapor content of the atmosphere and the temperature. The degree of refraction is measured by the receiver [Yunck *et al*, 2000].

#### 1.6.2 History of Radio Occultation

While GPS radio-occultation (RO) was first used by NASA to look at the atmosphere and ring structure of other planets in the 1960s, it was not applied to study the Earth's atmosphere until the mid 1990s when GPS satellites began orbiting in large enough numbers. RO allows for widespread measurement of temperature and water vapor within the atmosphere without needed to interact with the surface [Ware, 1996].

In 1991, the University Corporation for Atmospheric Research (UCAR) began a project, GPS/MET, to test RO in Earth's atmosphere. A modified GPS receiver, MicroLab 1, was launched into low orbit in April

1995 [Yunck, 2000]. The first temperature profiles from GPS/MET observations were constructed 13 days after launch. Despite several simplifying assumptions, the temperature profile over Ecuador was remarkably similar to a radiosonde profile taken 500km away [Ware, 1996]. GPS/MET was an “unqualified success.” Not only did it prove the concept of RO in Earth’s atmosphere beautifully, it provided many insights into how to better design the next occultation receivers. These early experiments made way for COSMIC and other RO projects to better and more widely measure quantities in the atmosphere [Yunck *et al*, 2000].

### 1.6.3 COSMIC Data

The COMSIC data product used in this analysis is ecmPrf. This provides the temperature, refractivity, water vapor pressure, latitude, and longitude for measurements taken at pressure surfaces in an atmospheric column. The measurements are taken at approximately every 50 hPa for the first, 200 hPa, and then every 100 hPa for the rest of the atmosphere. With roughly 2,000 soundings a day and ten years of data, COSMIC provides one of the best windows into global precipitable water vapor.

## 1.7 PREVIOUS RESEARCH

Bretherton *et al* [2004] found the relationship between precipitation and precipitable water vapor over tropical oceans but not over land. The researchers used the daily averaged TRMM precipitation measurements and daily averaged Remote Sensing Systems Inc. Special Sensor Microwave Imager (SSM/I) precipitable water vapor measurements. SSM/I uses microwaves to measure precipitable water vapor twice a day, local morning and local evening, providing a potentially more accurate average precipitable water vapor for the day than can be achieved with COSMIC. As discussed above, because of the interaction the microwaves have with land, no measurements can be taken over land using this technique. Both SSM/I and TRMM are gridded at a resolution of 0.25 x

0.25 degrees.

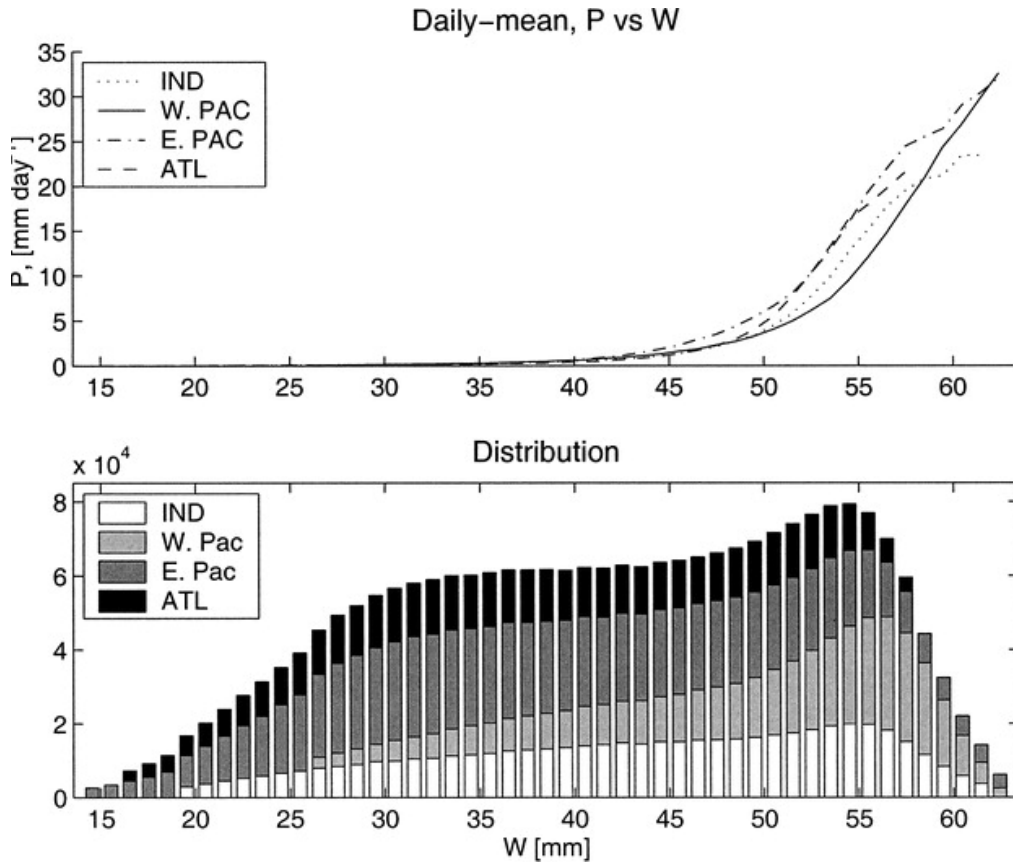


**Figure 3| Relationship Between Precipitation and Precipitation Water Vapor Over Tropical Oceans and Distribution. (Bretherton et al, 2004)**

As can be seen in Figure 2, they found an exponential relationship between the precipitation and precipitable water vapor that held for all four sections of the tropical ocean. As precipitable water vapor increased, the mean amount of precipitation increased rapidly at around 50mm. While there was a small variation in the curve among the four ocean segments they analyzed when looking at precipitable water vapor, this variation disappeared when precipitable water vapor was converted to relative humidity. Because of the expansive coverage of the data sets, even with only 3 years of data, *Bretherton et al.* were able to analyze many more data points than using COSMIC and TRMM allowed within my study. The benefit of using COSMIC and the progress this thesis makes

over Bretherton et al [2004] is the ability to look at precipitable water vapor measurements over land.

### 1.8 SUOMINET

To check the results from the COSMIC data, I used SUOMINET, another water vapor project by UCAR. Instead of satellite-based GPS occultation, SUOMINET uses ground-based sites. There are 10 sites over the Maritime Continent which took measurements for some portion of 2006 to 2015. Their locations can be seen in Figure 4 and the coordinates of their locations are in Table 1.

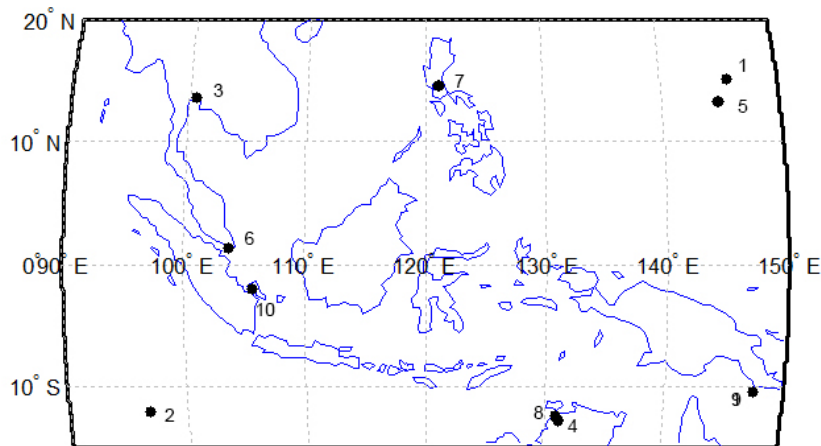


**Figure 4| Map of SUOMINET Station Locations.** Numbers correspond to the locations in Table 1

Station #	Latitude (°N)	Longitude (°E)
<b>1</b>	15.2297	145.7431
<b>2</b>	-12.1883	96.834
<b>3</b>	13.7359	100.5339
<b>4</b>	-12.8437	131.1327
<b>5</b>	13.4332	144.8027
<b>6</b>	1.3458	103.68
<b>7</b>	14.6357	121.0777
<b>8</b>	-12.4246	130.8916
<b>9</b>	-10.45	147.4253
<b>10</b>	-2.0609	105.6885

**Table 1| Coordinates for the SUOMINET stations**

All of the stations are positioned on land, but some of the islands they reside on are small enough that the MATLAB coast data does not identify them as land. The stations take measurements of column water vapor roughly every 30 minutes, which provides a very different data product from COSMIC where the measurements are distributed evenly over the earth. SUOMINET provides a wealth of information for a very few number of locations giving it very high temporal resolution but very poor spatial resolution. COSMIC, on the other hand, provides few measurements but for the entire globe giving it worse temporal resolution but considerably better spatial resolution.

## Chapter 2: Initial Analysis

### 2.1 GENERAL METHODS

#### 2.1.1 PRECIPITABLE WATER VAPOR COLUMN ANALYSIS

The precipitable water vapor is the total water within a column of the atmosphere. In this thesis, the water will be represented as a height. The height the water would be if all the water vapor in the column of atmosphere was converted to liquid water and brought to the surface of the earth. Within the atmosphere, water is contained almost entirely below the tropopause at around 150 hPa, the top boundary of the troposphere [Jacob, 1999].

Within each COSMIC sounding, measurements are taken at 21 different pressure heights, these constituting the atmospheric column. For each of the pressure heights, there is a location in latitude and longitude. Because the satellites move as they take measurements, the latitudes and longitudes of all points within a column are not perfectly equivalent. The first 10 measurements (1,000 hPa to 150 hPa) are integrated to get precipitable water vapor within the column. The latitude and longitude values used to represent the location of the COSMIC measurement is the average of the 10 latitudes and longitudes that correspond with the 10 measurements at each pressure surface along the column.

For each pressure surface, COSMIC provides the corresponding water vapor pressure. By knowing the total pressure and the water vapor pressure, we can calculate the mixing ratio of water in air using

$$C_{H_2O} = B \frac{e}{(P - e)}$$

where  $C_{H_2O}$  is the mixing ratio in kg of water/kg dry air,  $B$  is the ratio of molecular weight of water to molecular weight of dry air in g/kg, a

constant equal to 622 g/kg,  $e$  is the water vapor pressure, a quantity given by COSMIC, and  $P$  is the total atmospheric pressure.

By knowing the mixing ratio at each pressure surface, we can calculate the total amount of water vapor in a column. To calculate the amount of water vapor in each segment of column, first, the mass of air in the segment needs to be determined. The pressure difference between the top and the bottom of the segment is calculated and multiplied by the mass of the air per hPa, 10.2 kg/hPa. To establish the mixing ratio for the segment, an average mixing ratio between the two surfaces is taken. This is multiplied by the mass of the air to get the mass of the water in the segment. In order to calculate the height of the water, the mass of the air in a 1 m<sup>2</sup> area is divided by the density of water to find the height in mm.

### 2.1.2 TREATMENT OF THE TRMM DATA

The TRMM data is gridded at 0.25 x 0.25 degrees eight times a day in three-hour blocks. The 3-hour blocks are NASA's self imposed delineations. Each 3-hour block contains all of the TRMM observations taken 1.5 hours before and after but the metadata for the exact time the observations were taken is not provided. While there is not an observation for every 0.25 x 0.25 degree location every three hours, it is extremely close. For the TRMM data used in this thesis, 93% of the measurements that were needed, existed.

The completeness of the TRMM data set allowed me to look at the effect of narrowing and expanding the temporal resolution on the relationship between precipitation and precipitable water vapor. I looked at three different resolutions, one precipitation measurement (3-hour), three precipitation measurements (9-hour), and a daily averaged precipitation measurement.

The 3-hour analysis allows the closest thing to knowing what is the precipitation at the moment the precipitable water vapor measurement was taken. To match each COSMIC observation with the appropriate

TRMM observation, I found the closest spatial grid point within the TRMM data file that corresponded to the right time block. If that TRMM measurement existed, it was recorded with the COSMIC measurement, its COSMIC location, and the time the COSMIC measurement was taken.

To expand the temporal resolution, the precipitation measurements in the 3-hour blocks before and after the collocated measurement for the same spatial location were used. This 9-hour analysis allows for slightly more information about what is occurring during the time before and after the precipitable water vapor measurement was taken. The average of the valid precipitation measurements within those three measurements was calculated and recorded with the COSMIC observation.

To further expand the temporal resolution, the daily average of precipitation was used. This daily average allows to examine the effect the diurnal cycle has on the precipitation and precipitable water vapor relationship. For each COSMIC measurement, the average of the valid precipitation values within the eight precipitation measurements that constituted the day the COSMIC measurement fell within was calculated.

### 2.1.3 FINDING THE RELATIONSHIP BETWEEN PRECIPITATION AND PRECIPITABLE WATER

For each of the varied temporal resolutions, all of the measurements over the Maritime Continent were divided between land and ocean using the MATLAB coast line data. Each set of data (ocean and land) was then binned into mm wide segments and the average of precipitation for each bin is taken. Because of the difference in size of the number of observations over ocean and land, when deciding cutoffs for what values should be plotted, I needed to use a percent value instead of an absolute value. The precipitable water vapor mm wise segments with 1% of the data set or more. This corresponds to values between 15 mm and 65 mm which were then plotted.

### 2.1.4 BOOTSTRAPPING

To try to put some statistical bounds on the data, I used a technique known as bootstrapping. 20% of the data is deleted and then that same percentage of data points are duplicated and added back so the new data set remains the same size. The the same analysis is run on the data as if it were the original. This is repeated 1,000 times and allows for a measure of how robust the data is. If the data is well concentrated around one line, deleting 20% of the data and duplicating the same amount should have only a small impact on

## 2.2 DATA OVERVIEW

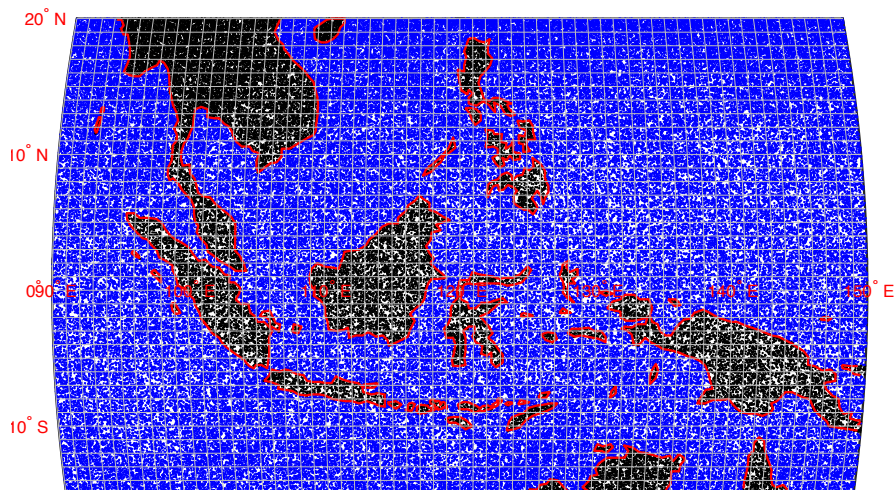


**Figure 5| Map of COSMIC Observations over the Maritime Continent**

The data range shown is from 2006 to 2015. Each dot indicates a COSMIC observation of precipitable water vapor. Black dots are observations of water vapor over land and blue dots are observations over ocean.

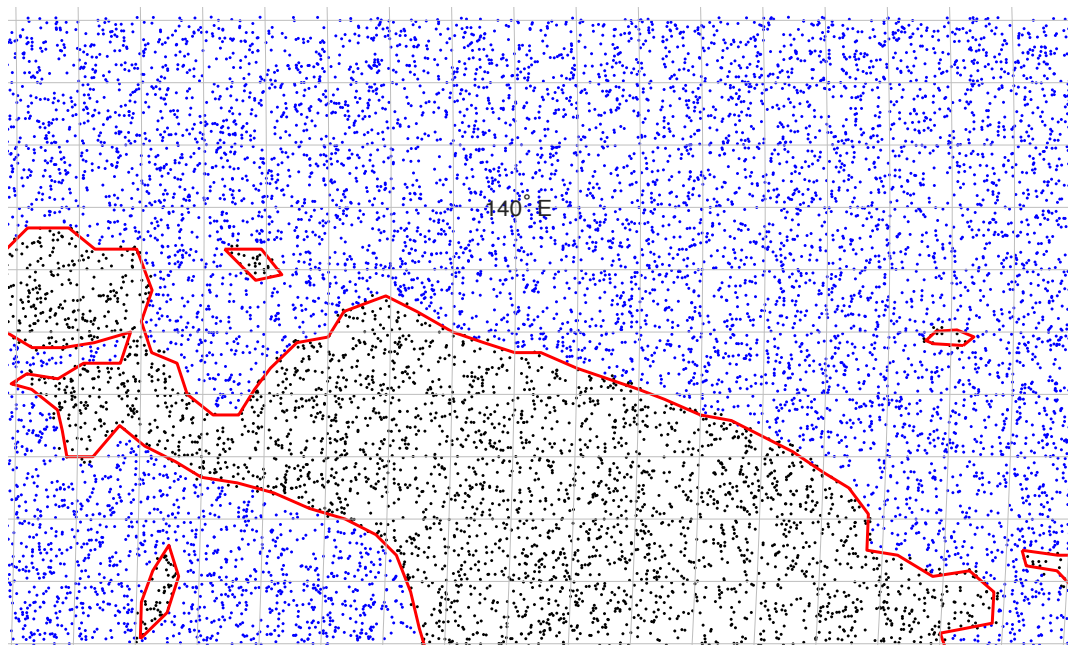


**Figure 6| Close up of a Section of Map of COSMIC Observations over the Maritime Continent** Displayed is a close up of 7°S to 3°N and 132°E to 149°E. The grid lines are spaced every at degree.

The overlap of the TRMM and COSMIC data sets allows for the use of almost ten years of data, April 23, 2006 to December 31, 2015. The total number of data points for all the TRMM-COSMIC analysis over the Maritime Continent is 158,013. The number of land data points is 30,635 (19%) and ocean data points is 127,378 (81%). As can be seen from Figure 5, the data points are well distributed over the area under examination. The close up in Figure 6 where each observation can be more clearly seen better displays the concentration of data points within the Maritime Contitnet.

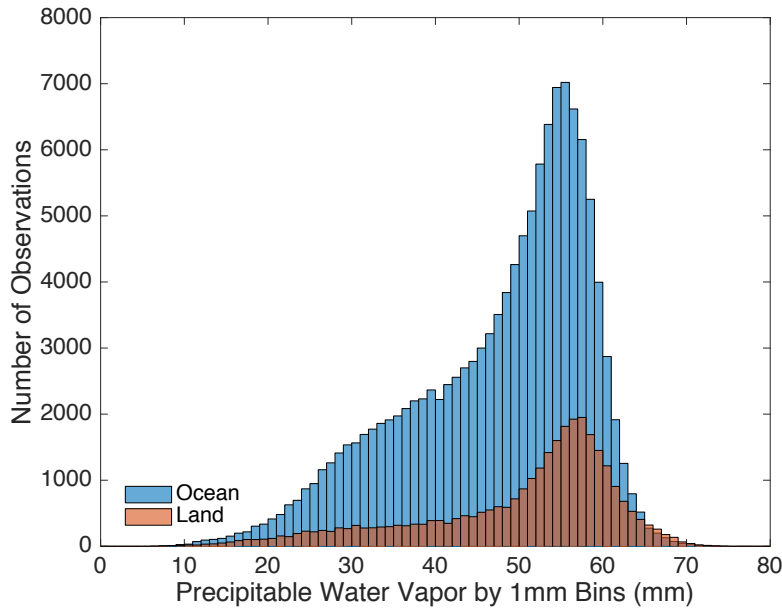


**Figure 7| Histogram of COSMIC Observations.** Number of COSMIC precipitable water vapor observations over the Maritime Continent divided between ocean and land separated into 1 mm bins.

The distribution of precipitable water vapor observations over land is more concentrated at a single peak than the ocean observations. While this can be seen in Figure 7, it is more clear in Figure 8. There are more observations of lower levels of precipitable water vapor over the ocean. The peak of precipitable water vapor for the land observations is also several millimeters higher than the ocean observations. This is consistent with the higher average precipitable water vapor observed over the land as can be seen in Figure 9.

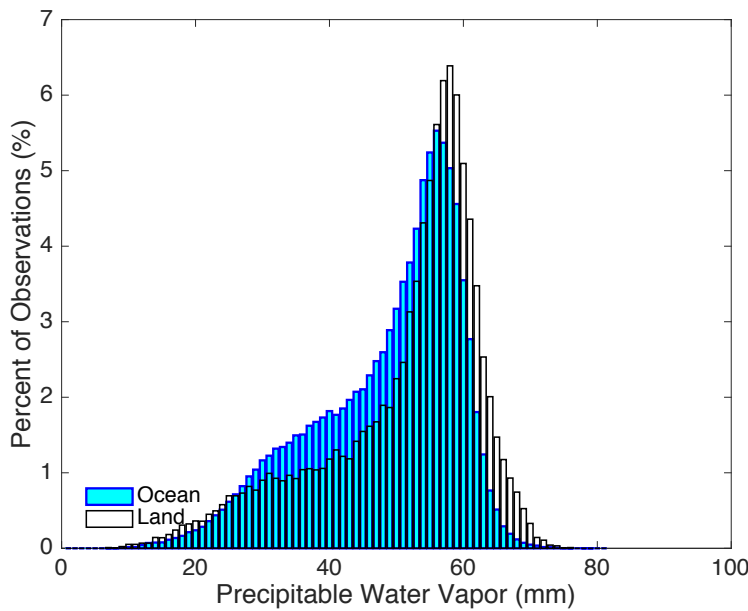


**Figure 8| Histogram of Percent of COSMIC Observations.**

COSMIC precipitable water vapor observations over the Maritime Continent separated into 1 mm bins as a percent of the total observations for each category, divided between ocean (black) and land (blue) separated.

The distribution of observations I found with COSMIC data is not fully consistent with similar precipitable water vapor distributions. *Bretherton et al [2004]* found a distribution that while had a small peak at the small value, roughly 55 mm, had a much more even distribution between 30mm and 55mm as can be seen in Figure 3. One explanation for the difference in distribution is the slight difference in area analyzed by both data sets. They split the tropical oceans ( $20^{\circ}\text{S}$  to  $20^{\circ}\text{N}$ ) into four sections, Indian, West Pacific, East Pacific, and Atlantic. The area I analyzed, the Maritime Continent, is partially contained within the Indian and West Pacific which had similar distributions. The area of highest precipitable water vapor is the Maritime Continent and the areas to the west and east both have lower precipitable water vapor contents as can be seen in Figure 9. Splitting the Maritime Continent between the Indian and

West Pacific was leads to neither area containing all of the high precipitable water vapor measurements that exist over the Maritime Continent, potentially diluting the strong high peak seen in Figures 7 and 8. There is also a sharp difference between the precipitable water vapor content above  $15^{\circ}\text{S}$  and between  $15^{\circ}\text{S}$  and  $20^{\circ}\text{S}$ . While *Bretherton et al.* included this area, I only analyzed between  $15^{\circ}\text{S}$  and  $20^{\circ}\text{N}$  making the high value of precipitable water vapor in that area more pronounced. *Bretherton et al.* also analyzed the distribution of relative humidity values because of the greater range of temperatures within the areas the researchers examined. The distribution of relative humidity has a slightly stronger peak at 77% relative humidity than it does at 54 mm.

### 2.3 Climatology Overview

To investigate the climatology related to precipitable water vapor and precipitation, to provide some verification of my code correctly interpreted the data, and to check the COSMIC precipitable water was within the realm of accepted possibilities, I used the COSMIC and TRMM data from 2006 to 2015 to make a number of maps of the Earth. I was also interested in the effect different seasons (boreal winter and summer) had on the average precipitable water vapor and precipitation.

#### 2.3.1 Methods

The maps are resolved to  $1^{\circ}$  by  $1^{\circ}$  for  $50^{\circ}\text{S}$  to  $50^{\circ}\text{N}$  across the entire globe. To plot the maps for precipitable water vapor, all of the COSMIC observations that corresponded to a TRMM observation within the  $1^{\circ}$  square for the time span of interest were averaged and then plotted. To plot the maps for precipitation, the same was done but for all the TRMM observations that corresponded to a COSMIC observation.

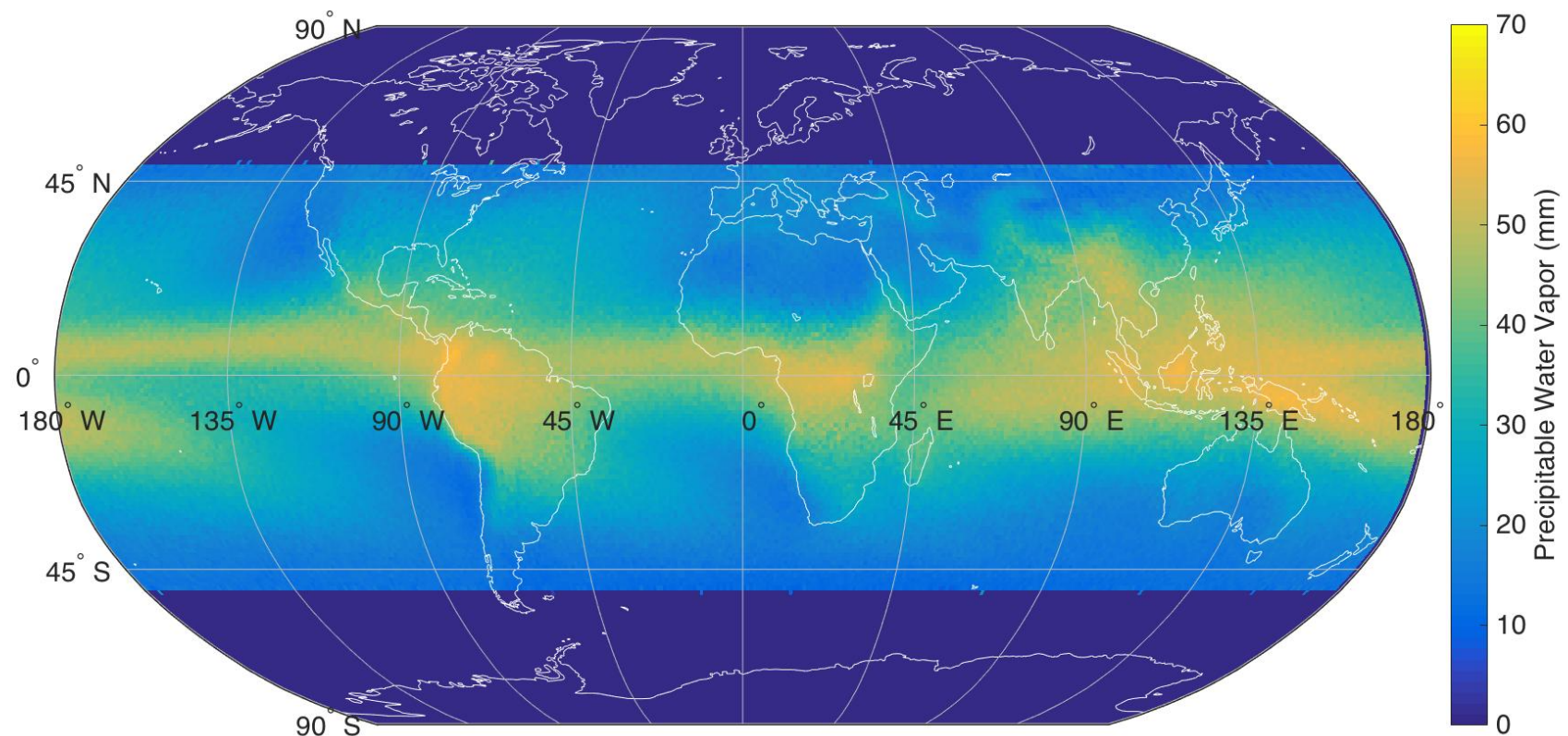


**Figure 9|Map of the Average COSMIC Precipitable Water Vapor**

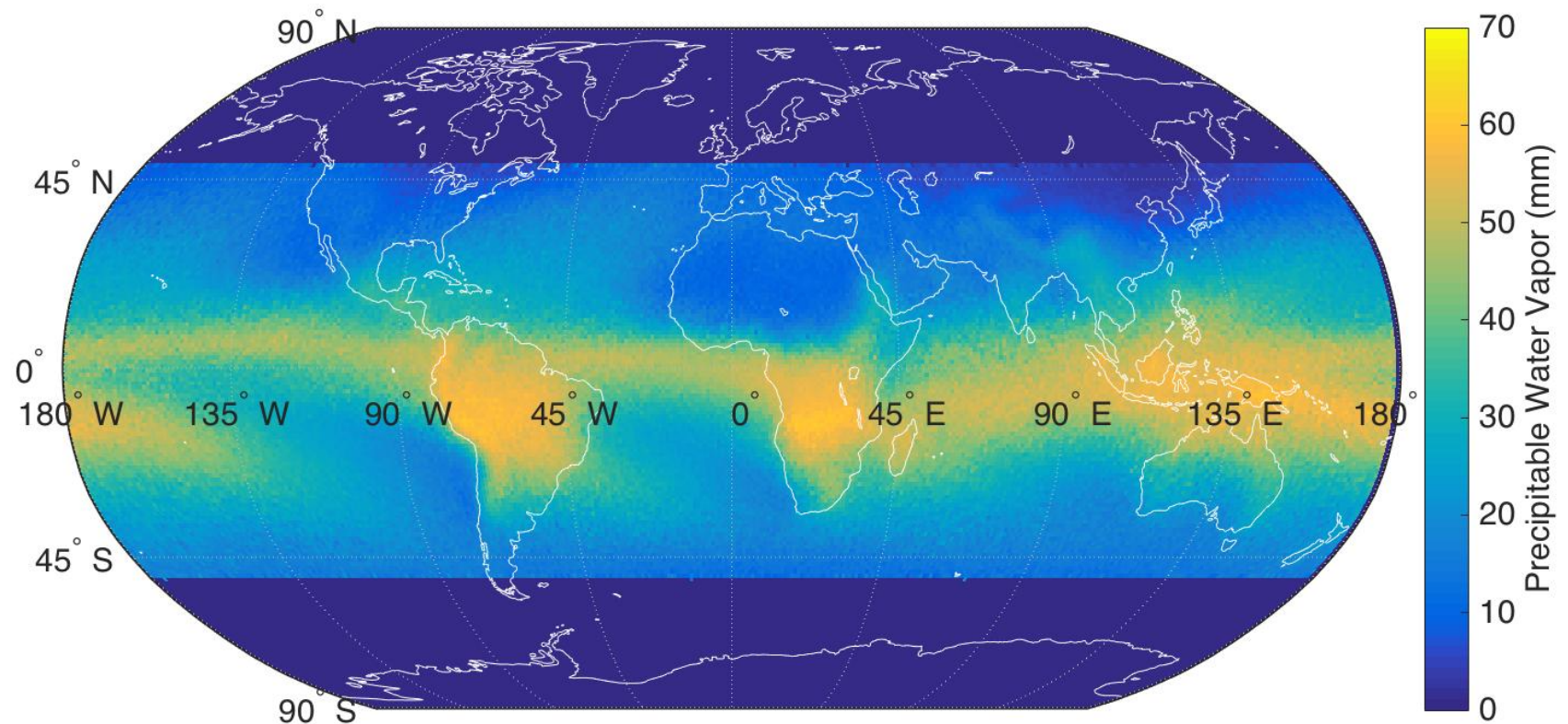


**Figure 10|Map of the Average Boreal Winter COSMIC Precipitable Water Vapor**

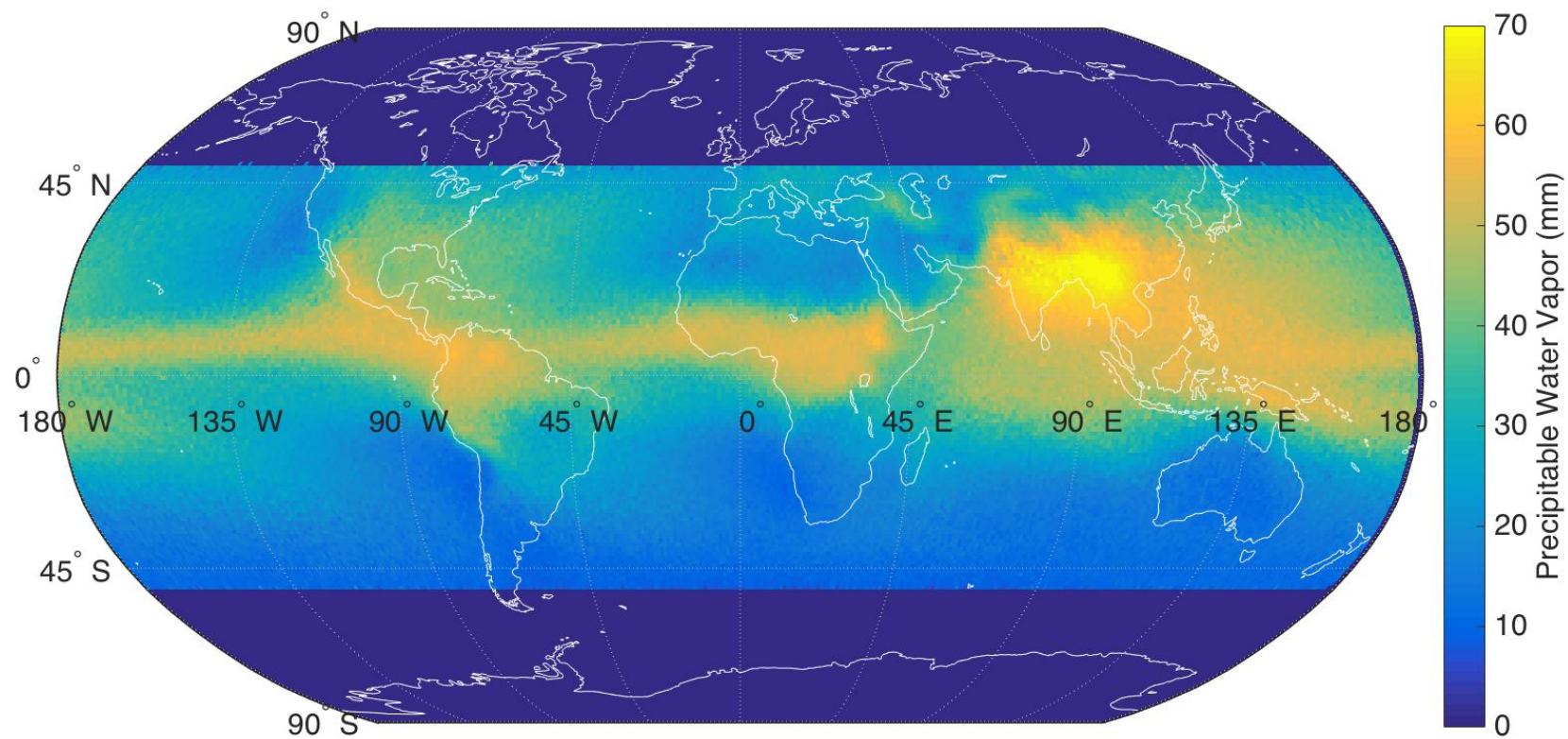


**Figure 11|Map of the Average Boreal Summer COSMIC Precipitable Water Vapor**

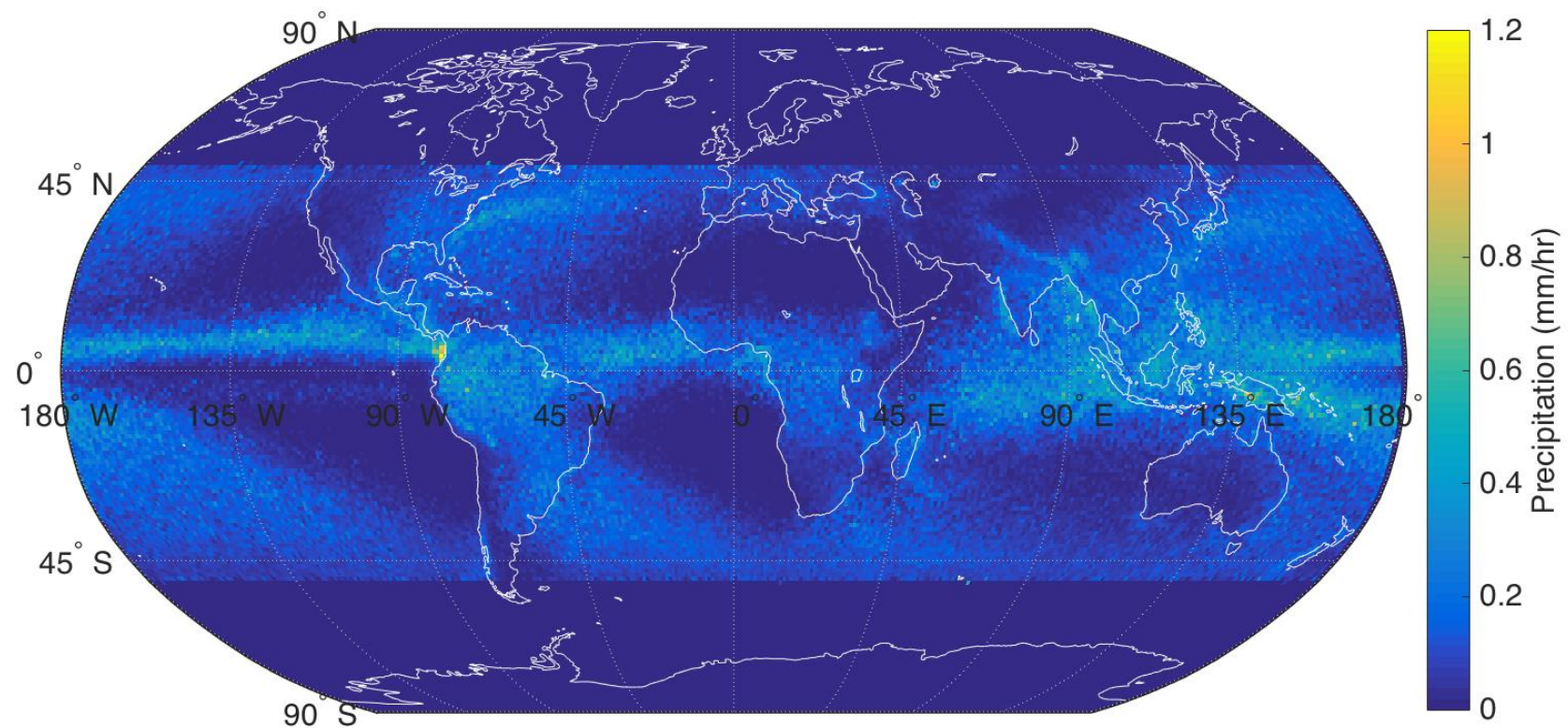


**Figure 12|Map of the Average TRMM Precipitation**

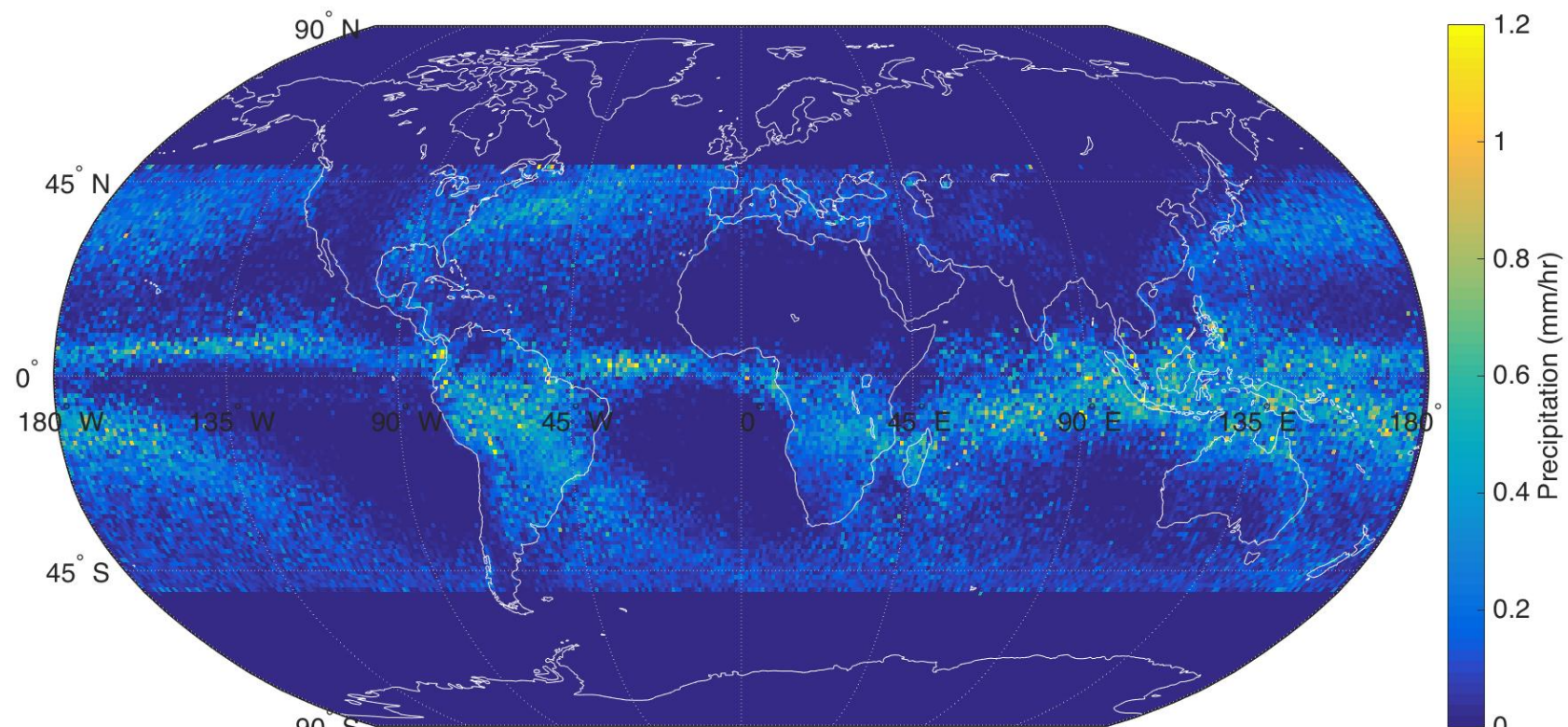


**Figure 13|Map of the Average Boreal Winter TRMM Precipitation**

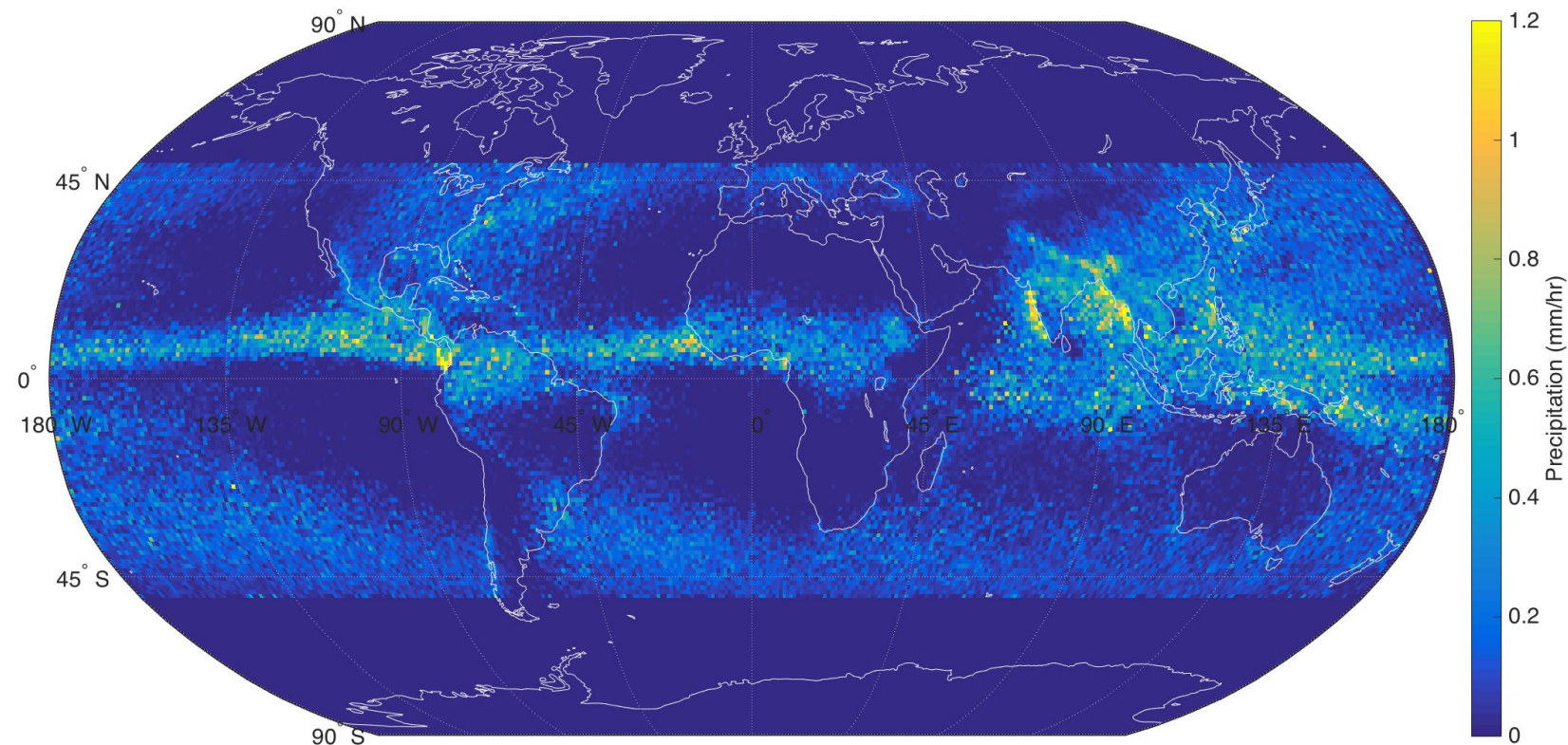


**Figure 13|Map of the Average Boreal Summer TRMM Precipitation**

### 2.3.2 Results

The maps came out as was expected. There is both more precipitation and precipitable water in boreal summer over the Maritime Continent. The high precipitation and precipitable water vapor is clear along the Inter Tropical Convergence Zone as is expected. As can be seen clearly in the boreal summer map of precipitation (Figure 11), the Maritime Continent is the area of the Earth with the highest precipitation.

## 2.4 DIURNAL CYCLE

One of the largest differences between the ocean and the land is the difference in heat capacity between the two. Because of the significantly higher heat capacity of water, the change in heating due to the sun has a smaller impact and the variance of temperature is lower. This leads to a more severe diurnal cycle over land than over the ocean. Because of the potential for a large difference in the diurnal cycle, I was interested to see if there was a strong effect the diurnal cycle had on water vapor and for precipitation over land and ocean.

### 2.4.1 PRECIPITABLE WATER VAPOR

To investigate the effect of heating on the amount of precipitable water vapor, I plotted the diurnal cycle of precipitable water vapor for the COSMIC data. I divided the data between land and ocean. I then converted the data from UTC—the time zone used in the data set, to local time. I subsequently averaged each of the hour-long bins to plot the diurnal cycle of water vapor.

Because all SUOMINET data for the Maritime Continent is collected at only 10 distinct stations, I plotted the individual stations' diurnal cycle using the same method as outlined above.

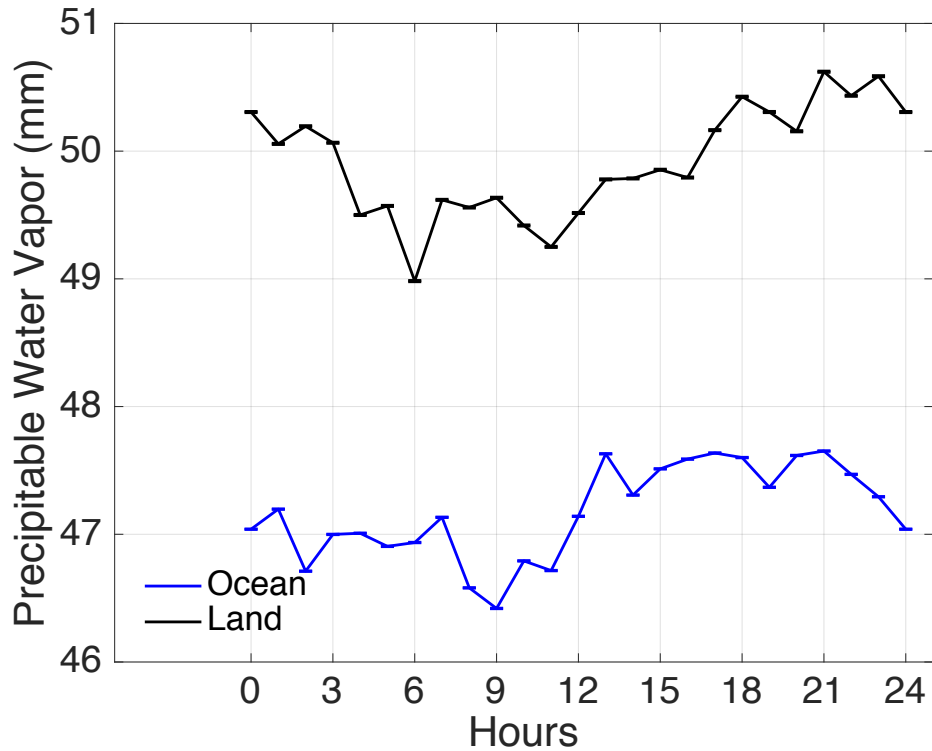


**Figure 15|Diurnal cycle of COSMIC Precipitable Water Vapor** divided between observations over land and ocean. The measurement at hour 24 is the same as hour 0 to allow for a complete cycle.

The diurnal cycle of precipitable water vapor over land is slightly stronger and more pronounced than the diurnal cycle over the ocean, but not as much as was expected, shown in Figure 15. The average precipitable water vapor over land is around 3mm higher than over the ocean. This can also be seen in Figure 9 showing a map of the average precipitable water vapor.

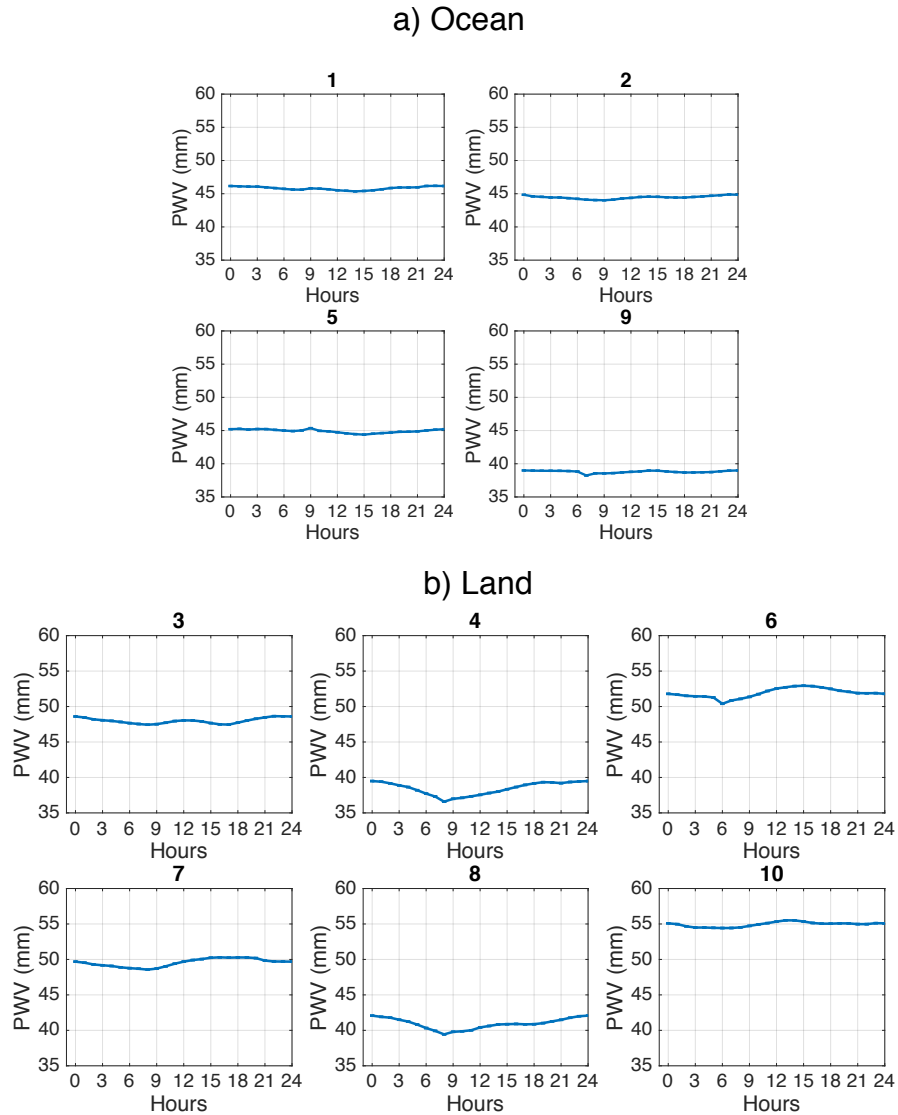


**Figure 16|Diurnal cycle of each SUOMINET station precipitable water vapor.** The numbers correspond to the station coordinates in Table 1 and Figure 4 indicates where the stations are located on a map of the Maritime Continent. The measurement at hour 24 is the same as hour 0 to allow for a complete cycle to be plotted. a) The stations that are designated ocean stations. b) Stations that are designated land stations.

The diurnal cycles of precipitable water vapor observed at the SUOMINET stations contain many of the same elements of the average diurnal cycle seen in COSMIC data. Neither the ocean nor the land

stations exhibit strong changes in precipitable water vapor over the course of a day though Stations 4 and 8 both show more change over the course of a day than the rest of the stations.

#### 2.4.2 PRECIPITATION

To look at the diurnal cycle of precipitation, all of the TRMM measurements taken between 2006 and 2015 were used, not just the the measurements with a corresponding COSMIC measurement leading to a much larger number of observations and much smoother plots.

Because the TRMM data is taken within a three-hour block, the greatest resolution that can be achieved for the diurnal cycle is three hours. The TRMM data was converted from UTC to local time, binned within the three-hour blocks, and these blocks were averaged.

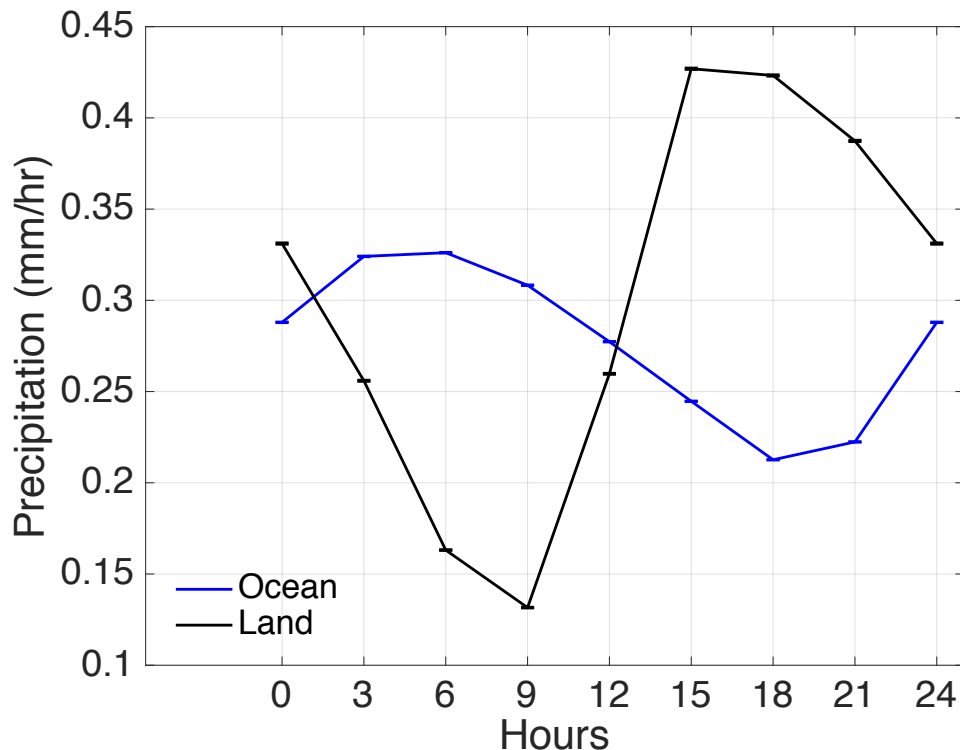


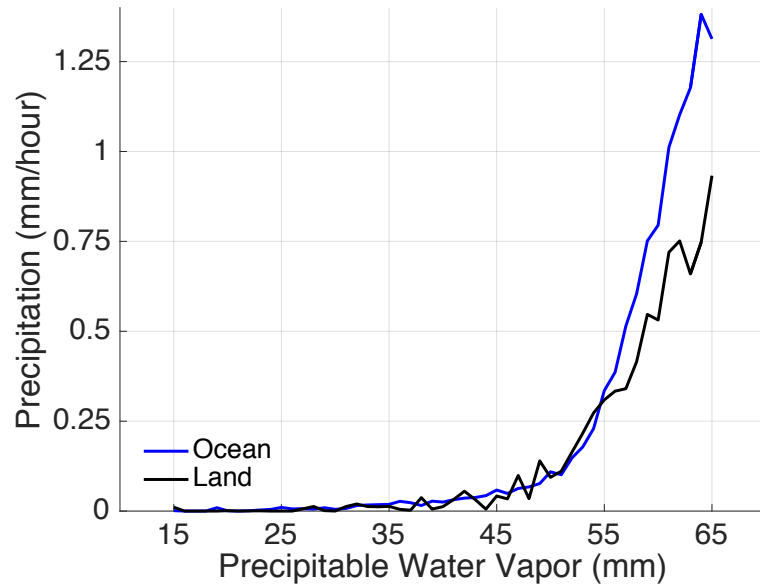
**Figure 17|Diurnal cycle of TRMM Precipitation Observations**  
They are divided between land (black) and ocean (blue). The measurement at hour 24 is the same as hour 0 to allow for a complete cycle to be plotted.

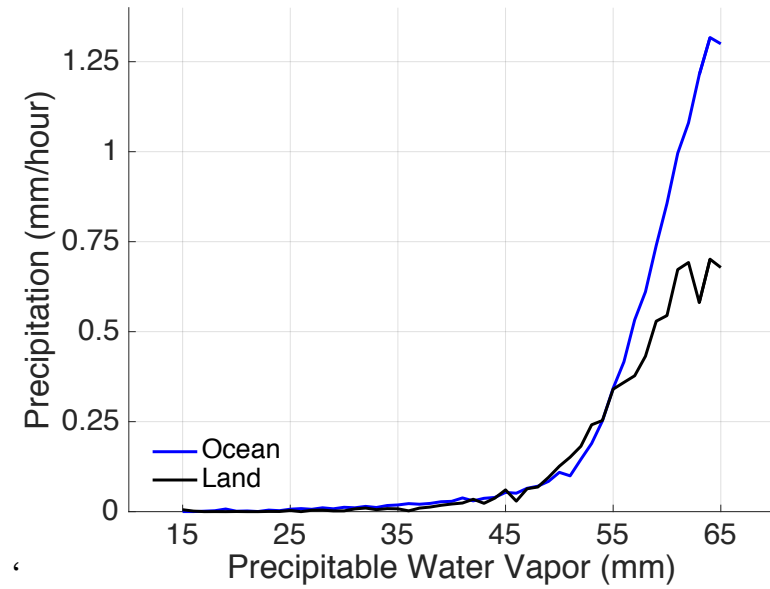
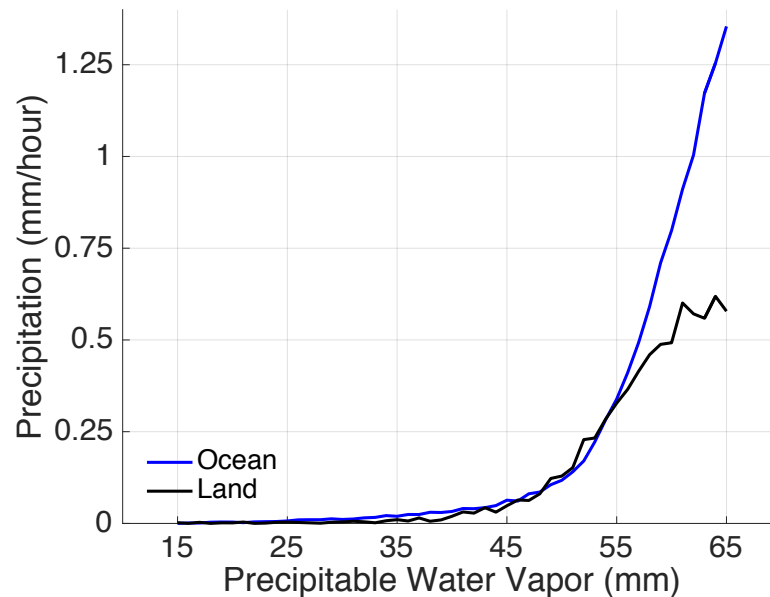
The diurnal cycle of precipitation for both the ocean and the land are much clearer than for precipitable water vapor. The diurnal cycle of precipitation for the land is much stronger with a steep growth in amount of precipitation between 9:00 and 15:00. It remains high through 18:00 before it begins to fall throughout the rest of the evening and early morning.

The diurnal cycle for the ocean is considerably weaker and has a phase lag of  $\pi$ , reversing the progression in time. Precipitation over the ocean is highest between 3:00 and 6:00, falls gradually across the entire day to reach the lowest amount of precipitation at 18:00 and then rises gradually throughout the night.

## 2.5 RELATIONSHIP BETWEEN PRECIPITATION AND PRECIPITABLE WATER VAPOR

**a) 3-Hour**



**b) 9-Hour****c) Daily**

**Figure 18|Plot of the Relationship Between Precipitation and Precipitable Water Vapor** a) Mean 3-hour TRMM precipitation in 1mm bins of COSMIC precipitable water vapor. b) Mean 9-hour TRMM precipitation in 1mm bins of COSMIC precipitable water vapor. c) Mean Daily TRMM precipitation in 1mm bins of COSMIC precipitable water vapor

Similar to relationship found by *Bretherton et al.* in 2004, the relationship between precipitation and precipitable water vapor over the ocean is exponential with a sharp increase in precipitation as precipitable water increases. Even as the temporal resolution changes, the relationship over the ocean remains nearly the same. This can be seen in the near identical plots over the ocean in Figures 18a, 18b, and 18c. One difference between the plots as the temporal resolution expands is the noise within the plot decreases with decreased resolution.

The relationship between precipitation and precipitable water vapor over land appears to be much more complicated. Between 0 and 55mm, the relationship between precipitation and precipitable water vapor for oceans and land is the same. The plots lie on top of each other. But after 55mm the two relationships diverge. While interesting to note but appears coincidental, 55 mm of precipitable water vapor is where the peak of observations is for the ocean data and just slightly lower than the peak for land. Currently, there is no reason to think those two facts are linked.

For each temporal resolution, the increase in precipitation as precipitable water vapor increases is less severe than it is over the ocean. The plots become more different from each other as the temporal resolution is increased. For the 3-hour analysis (Figure 18a), while there is a clear difference in the relationship between land and ocean, it appears to be shifted as opposed to fundamentally altered. In the 9-hour analysis (Figure 18b), a cut off appears to start developing around 0.7 mm/hr of precipitation. The relationship at the higher values of precipitable water vapor is no longer exponential. In the daily analysis (Figure 18c), the cut off becomes much more clear. While at 65mm of precipitable water vapor, the average daily precipitation over the ocean is 1.4 mm/hr, over land it is just over 0.6 mm/hr.

From the weak diurnal cycles of precipitable water vapor over the ocean and the land (Figure 15), it appears that precipitable water vapor

does not change in a reliable pattern across a day. This is not to say that precipitable water vapor does not change within a day; there is just not a consistent pattern.

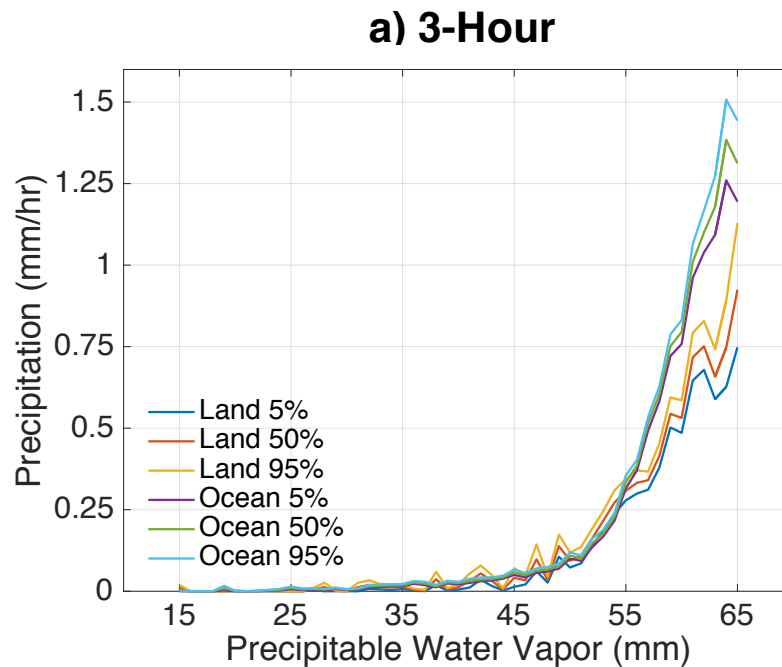
While divining a cause by looking at effects is challenging, one potential narrative to explain the plots is when there is high precipitable water vapor over the ocean, it rains a lot and it continues raining for the full day and the precipitable water vapor does not drop. This can be seen by the consistency of Figures 18a, b, and c. When the precipitation is averaged over the entire day, there the same amount of precipitation corresponds with the same level of precipitable water vapor. This would only occur if, on average, the rate of precipitation stayed fairly constant across any given day. This is partially corroborated by the weak diurnal cycle seen in ocean precipitation (Figure 17).

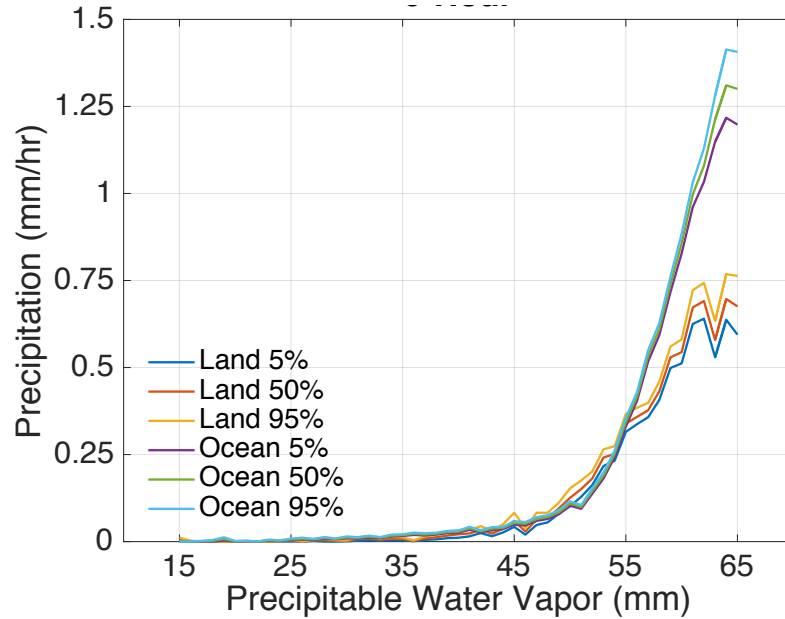
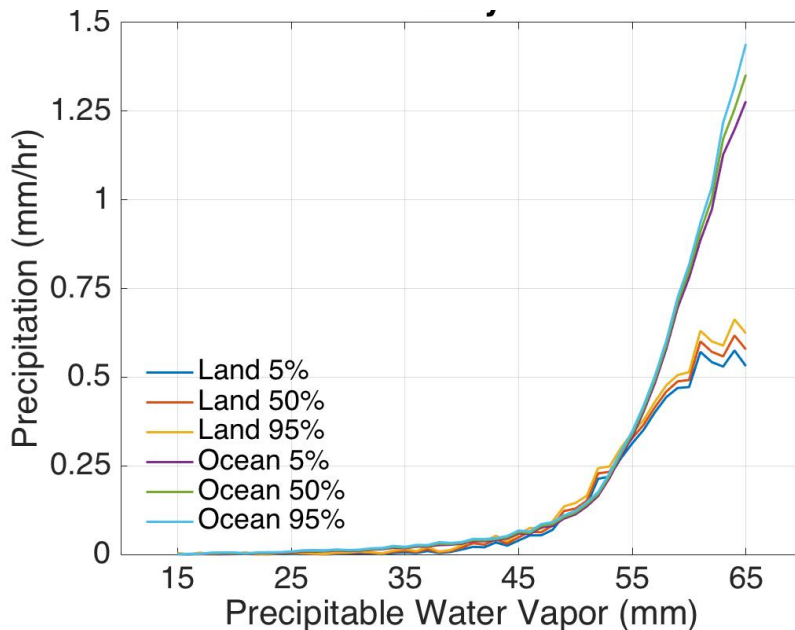
Over the land a different trend is observed for high levels of precipitable water vapor. When looking at the Figure 18a, the average amount of precipitation for a corresponding amount of precipitable water vapor is smaller over the land than over the ocean; however, it is more similar to a shifted exponential curve than to a curve that is flattening. As more precipitation measurements are averaged to cover a wider amount of time, the curve begins to flatten. The amount of average precipitation falls for measurements of high precipitable water vapor as more of the day is included. This means for a given measurement of 60 mm of precipitable water vapor, the precipitation measurement closest in time was, on average, the highest value. When more of the day is included, the average amount of precipitation for that 60 mm observation decreases. This can be explained by the stronger precipitation diurnal cycle. Over the course of a day, precipitation fluctuates. We know that as high amounts of precipitation occur over land, the precipitable water vapor also falls, because if there were high precipitable water vapor measurements with low precipitation, Figure 18a would look more like the daily averaged. But since, when precipitation is averaged, the level of precipitation falls, it would seem like the precipitable water vapor must also be falling.

If this explanation for the change in precipitation over land with a change in temporal resolution is true, it would follow that there was a diurnal cycle in precipitable water vapor. While it appears that there is a weak diurnal cycle, it is challenging to conclusively say from this data set because of the noise in the graph.

This has potential implications for the convective weakening of the MJO seen over the Maritime Continent. The change in temporal resolution and the difference in the relationship of precipitation and precipitable water vapor between the ocean and the land seen above indicates the high frequency forcing, relative to the MJO, that might be disturbing the convection within the MJO. The Maritime Continent is approximately 6500 km across at the equator and in the course of a day, moving at 5 m/s, the MJO will move 430 km. This means it makes approximately 15 days for the MJO to cross the Maritime Continent.

## 2.6 STATISTICAL BOUNDS ON RELATIONSHIP



**b) 9-Hour****c) Daily**

**Figure 19| Bootstrapped Plots of Relationship Between Precipitation and Precipitable Water Vapor.** All plots show 5, 50, and 95% of 1000 runs with 20% replacement of data. a) Plot of 3-hour TRMM precipitation b) Plot of 9-hour averaged TRMM precipitation c) Plot of daily averaged TRMM precipitation.

The relationships between precipitable water vapor and precipitation found in the Figure 19 are fairly robust. The 95% confidence bounds for the relationship are close together and the ocean and land lines do not overlap. This is especially true when looking at a daily average of precipitation (Figure 19c) where the 95% confidence bounds are almost on top of each other. The confidence interval gets smaller with more precipitation values averaged.

## Chapter 3: SUOMINET Analysis

In an effort to use another precipitable water vapor data set to verify the findings from the COSMIC TRMM analysis, I used the SUOMINET precipitable water vapor data. While vastly different from COSMIC in temporal and spatial resolution, it allows for some confirmation.

### 3.1 METHODS AND RESULTS

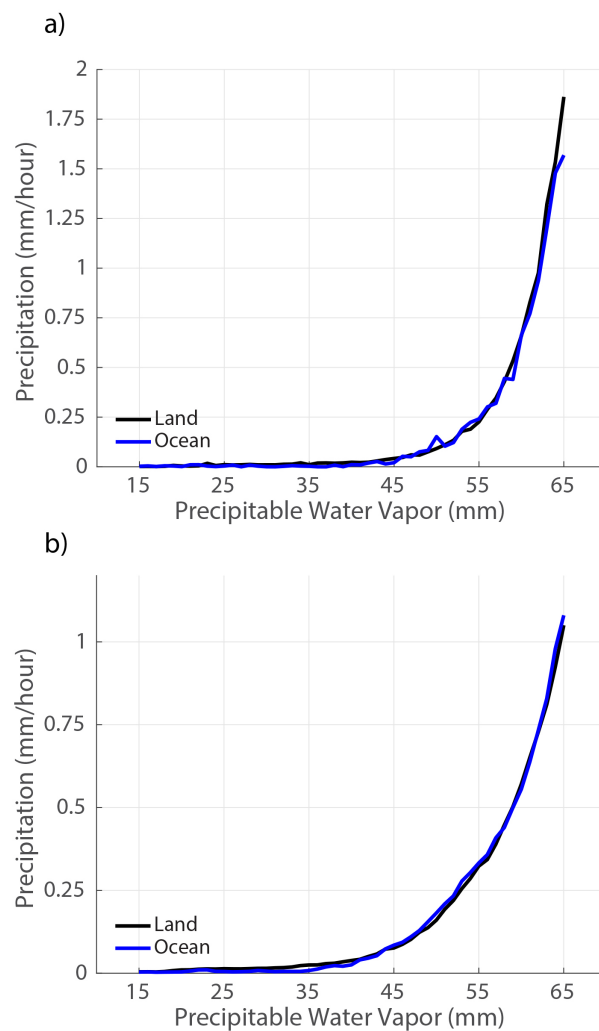


**Figure 20|Plots of SUOMINET Analysis** a) Three hour average of SUOMINET with TRMM 3-hour measurement b) Daily averaged TRMM precipitation with each SUOMINET measurement.

I analyzed the SUOMINET data in two ways. The first analysis took SUOMINET measurements of precipitable water vapor taken within the three-hour blocks of TRMM measurements and averaged them. They were then plotted with the TRMM measurements of precipitation for the same block of time. This analysis can be seen in Figure 20a. The plots of ocean and land are nearly identical in this plot, in great contrast to what is seen in the COSMIC analysis. Both land and ocean appear to have the same precipitable water vapor to precipitation relationship seen over the ocean in the COSMIC analysis.

The second analysis was done in the same manner as the daily averaged precipitation and COSMIC analysis because it was the relationship that saw the greatest difference between ocean and land. Each SUOMINET precipitable water vapor observation was treated as an instantaneous measurement paired with a daily averaged TRMM precipitation measurement for that same location. This plot can be seen in Figure 20b. Once again, the ocean and land plots lie almost exactly on top of each other.

### 3.2 COMPARING SUOMINET AND COSMIC

When first realizing the SUOMINET analysis did not corroborate the COSMIC analysis, I wanted to verify the COSMIC data and SUOMINET data had the same or similar observations for measurements taken in the same place at the same time. I looked at COSMIC data points within 1 degree latitude and 1 degree longitude of a SUOMINET station. Since the SUOMINET measurements are taken every 30 minutes, temporally, the COSMIC and SUOMINET data points are not more than 15 minutes apart. There were roughly 2,000 overlapping data points.

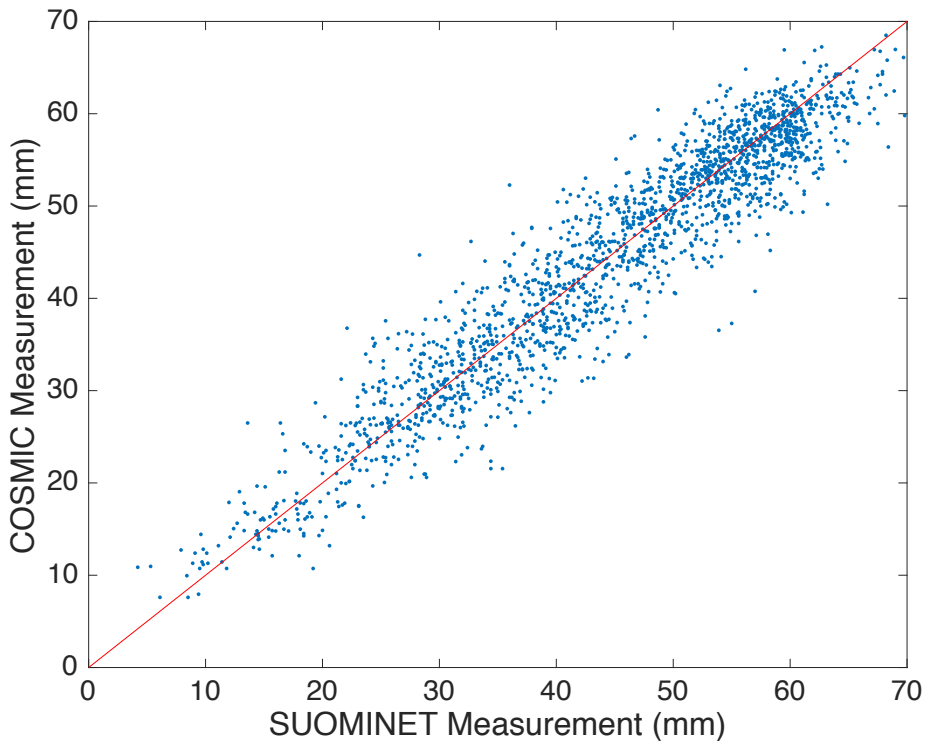


**Figure 21| Comparison of Close SUOMINET and COMSIC Measurements.** The red line lies at  $x = y$  and if the two measurements were exactly the same, they would lie along this line.

Overwhelmingly, the two measurements of precipitable water vapor are very similar or the same. But there is 3% of the data where the difference between the two measurements was more than 25% different from the average of the two measurements. While a small percent, it is still troubling that the two measurements would be so different.

To better understand what might cause this small percent of very different values, I examined the relationship between the difference in measurement and the distance between where the two measurements were taken. I plotted the distance in kilometers against the difference in between the two measurements. Surprisingly, there is a very weak correlation between distance the two measurements were taken and the difference in measurement of precipitable water vapor. I expected that the measurements taken closer together to be more similar to each other.

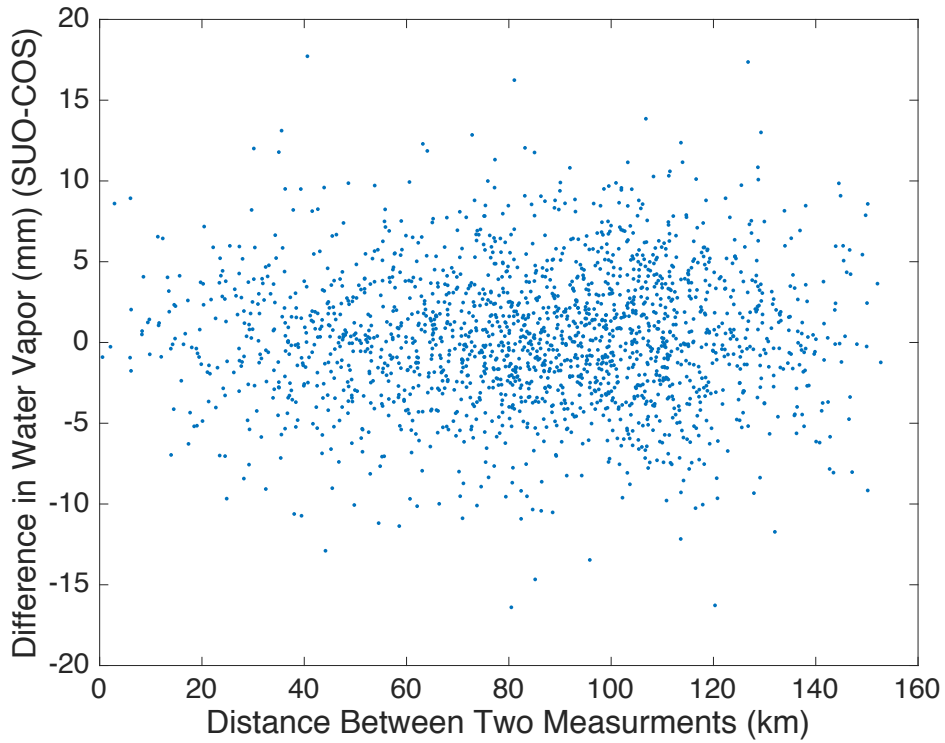


**Figure 22|Difference Between SUOMINET and COMSMIC by Distance**

One explanation for the disparity in the measurements and the lack of distance dependence may be related to how GPS RO works. The measurements at different pressure heights are not all perfectly on top of each other. Over the course of the pressure surfaces I use to calculate precipitable water vapor, the position of the measurement changes on average by a slightly more than a degree between the first and last measurement. The average of all of the pressure surface coordinates is the value that is used to as the location of the measurement. This introduces a significant error for looking at distance dependence within the small radius I examined. However, the concern with taking a larger radius is it begins being a test for how close are precipitable water vapor values in a certain area and not a test of the accuracy of the measurements taken by COSMIC and SUOMINET.

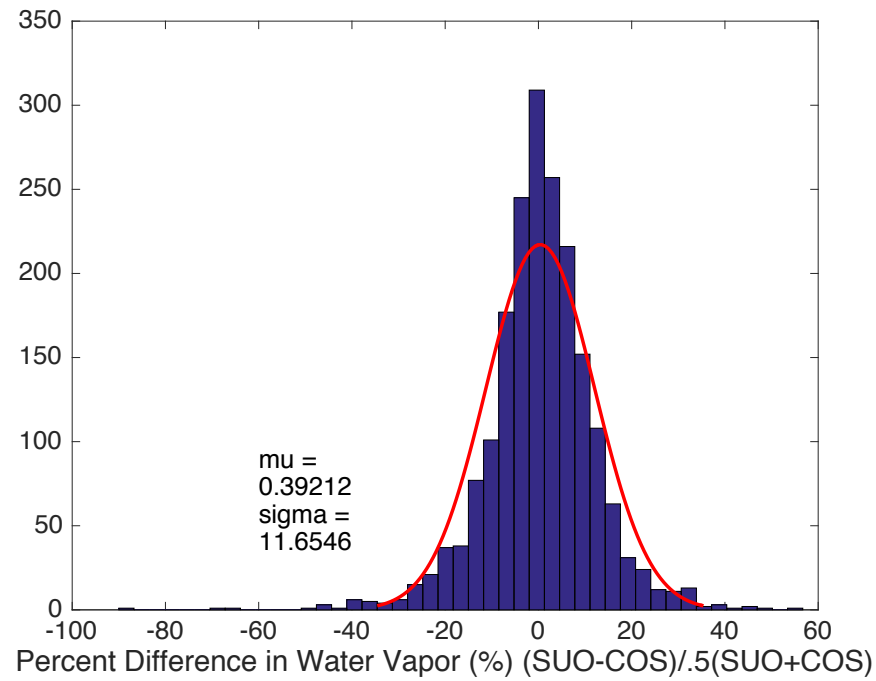


**Figure 23|Histogram of Percent Difference of COSMIC and SUOMINET Measurements**

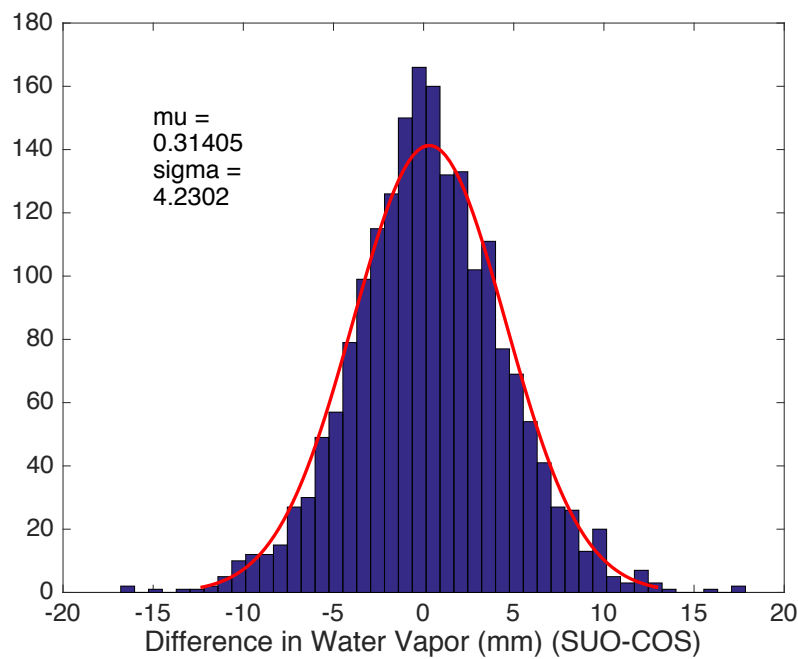


**Figure 24|Histogram of Difference in Measurement Between COSMIC and SUOMINET**

Luckily, the difference in the two measurements does not have a negative or positive bias with the average at 0.314 mm difference or a difference of 0.4%. The histograms of the absolute difference and percentage difference both fit a Gaussian distribution well. For a random distribution of differences, this is what would be expected.

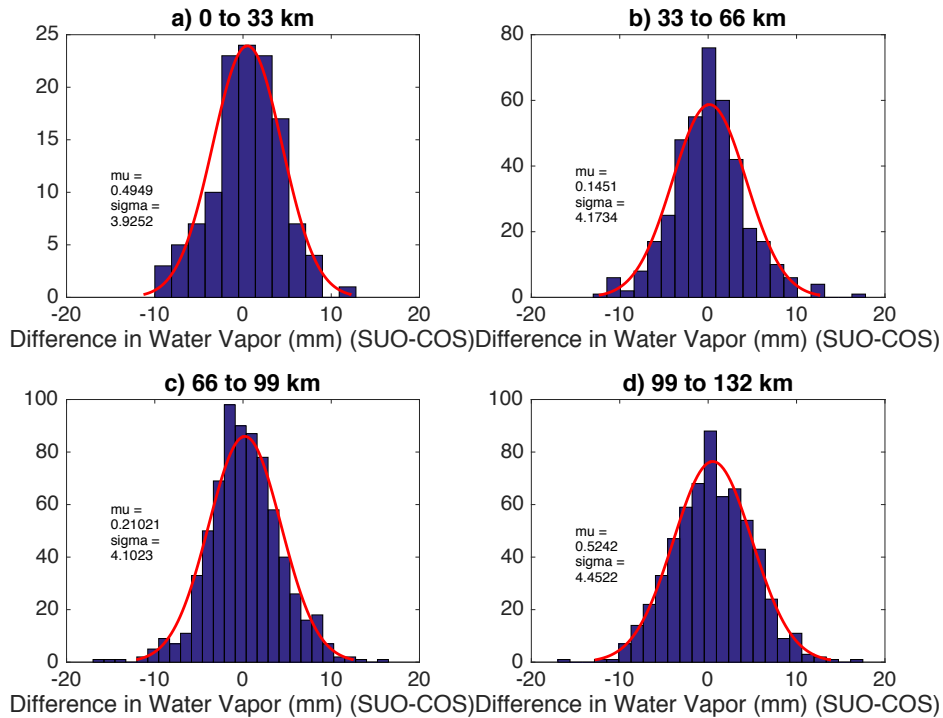


**Figure 25|Histograms of Difference in COSMIC and SUOMINET Measurements by Distance**

The four graphs in Figure 25 look at the distribution of differences at different intervals between the measurement distance. The first graph is measurements taken closer than 33 km to each other, the second is measurements taken between 33 and 66 km away from each other, the third between 66 and 99 km, and the fourth between 99 and 132 km.

Each of these four distributions look very similar to each other. The parameters of the Gaussian distributions, mu and sigma, do not vary

much between the four plots. There is a slight broadening of the plots at the distance increases but it is not significant.

## Chapter 4: Distance From A Coast

### 4.1 MOTIVATION

While there was a small number of COSMIC and SUOMINET measurements that did not adequately match up, this does not explain the difference in the relationship between precipitation and precipitable water vapor for the two data. One possible explanation for this failure is the location of the SUOMINET stations. All of the stations are on land but some of them are so small that the MATLAB coast program counts them as ocean. The stations that are designated at land are all very close a coastline. This can be seen in Figure 1.

### 4.2 METHODS

To find the distance for each land point to the nearest coast, I used MatLab code from Dan Chavas of Purdue University he made available online. To verify the code's functionality, I used the code to calculate the distance to the nearest coast of 10 different land points distributed over the Maritime Continent. Then used Google Earth to calculate the distance to the nearest coast. The two sets of values were consistent indicating the code was functional.

### 4.3 DATA OVERVIEW

To examine whether the difference in distance from a coast could explain the difference in the relationships between precipitation and precipitable water vapor ability of this to explain why the SUOMINET and COSMIC plots are so different, I divided the COSMIC land data points into thirds from their distance from a coast. The first group is within 38km of a coast. The second group is between 38 and 128km of a coast, and the last group is more than 128km from a coast. The spatial distribution of these segments is represented in Figure 26. Because of the even distribution of data over the entire Maritime Continent (Figure 5), it is a fair assumption

that a third of the land mass corresponds to a third of the COSMIC observations.

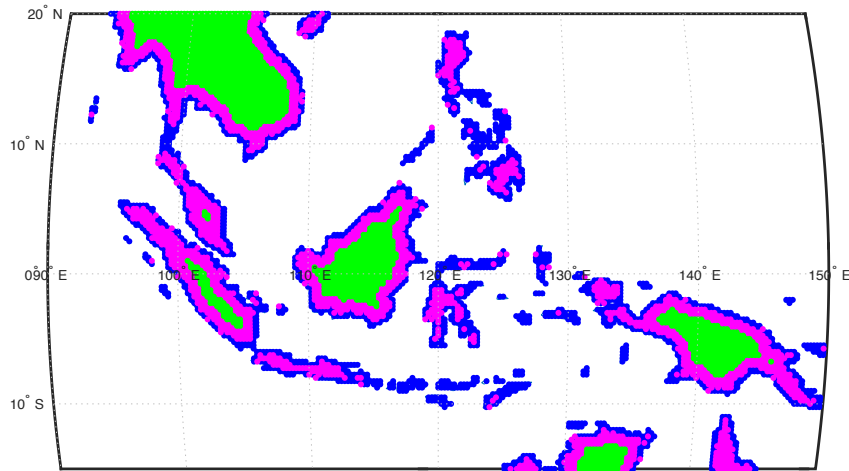


**Figure 26|Map of the Land Divided into Distance From a Coast.**  
Blue is within 38km of a coast, pink is between 38 and 128km of a coast, and green is more than 128km from a coast.

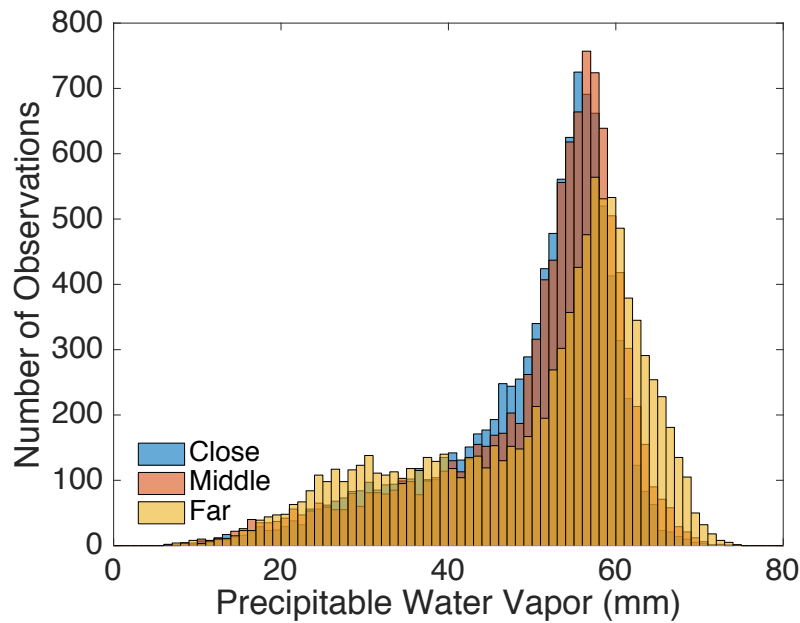


**Figure 27|Distribution of COSMIC Observations Over Land Divided by Distance From a Coast.** Land close to a coast (within 38km), a middle distance from a coast (between 38 and 128km), and a far distance from a coast (more than 128km).

Looking at the distribution of the water vapor measurements by distance from a coast, measurements taken within 38km and between 38 and 128km of the coast look very similar to each other compared to the measurements taken more than 128km from a coast. The group farther from the coast has a wider range of values. There are more small precipitable water vapor (20-30mm) measurements and more large measurements (65-70mm). Consequently, the peak of the histogram is lower. The peaks of the three sections of data are very close to each other. At less than 38km, the peak is at 56mm of precipitable water; between 38 and 128km, the peak is at 57mm; and at greater than 128km, the peak is at 58mm.

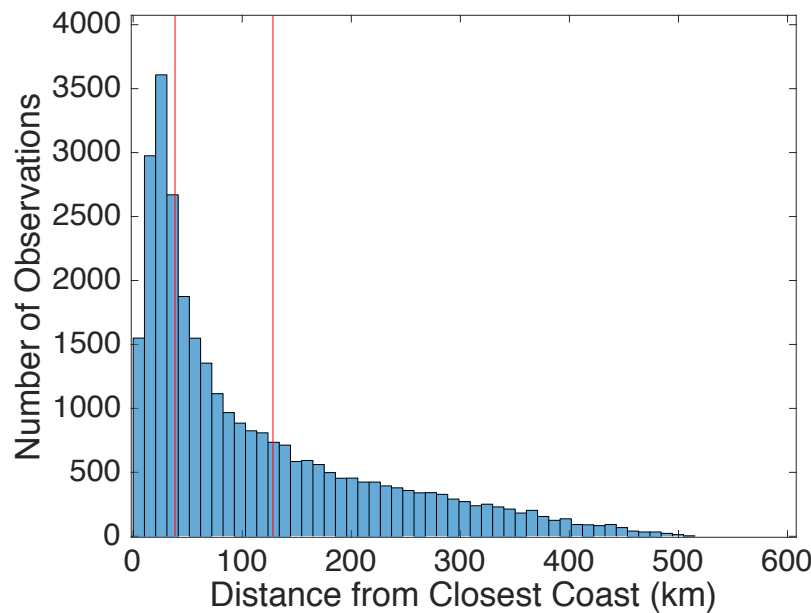


**Figure 28|Distribution of the Distance from Coast of COSMIC Observations.** The red lines demarcate the thirds of the data, 33% is at 38km and 67% is at 128km.

## 4.4 DUILRNAL CYCLES

### 4.4.1 PRECIPITABLE WATER VAPOR

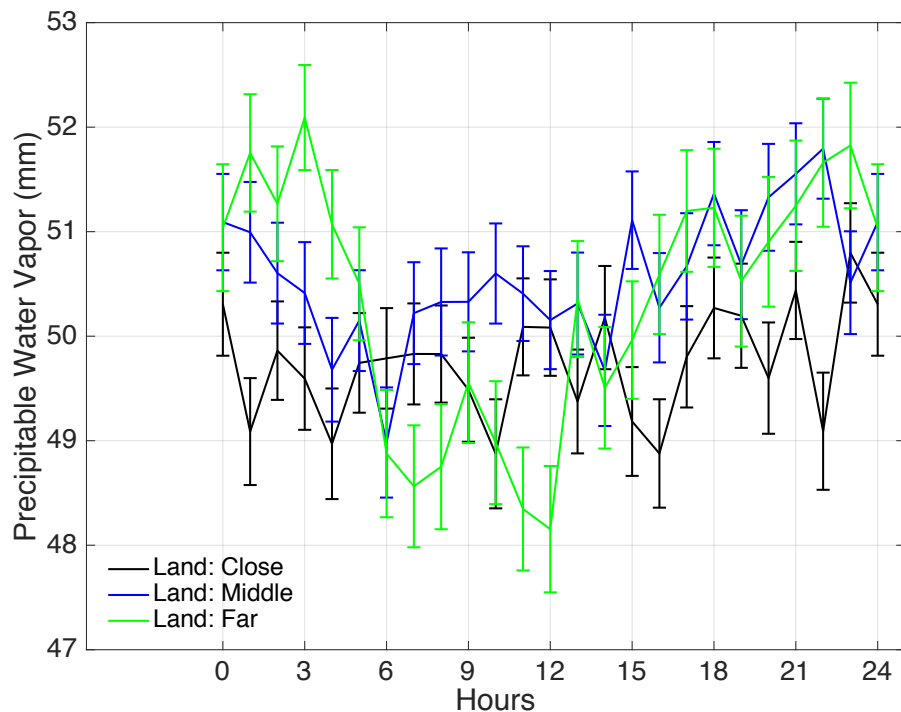


**Figure 29|Diurnal Cycle of COSMIC Observation by Distances From a Coast.** The measurement at hour 24 is the same as hour 0 to allow for a complete cycle to be plotted.

To see whether part of the diminished land diurnal cycle is a muddling of the ocean and land signals, the land was divided into three groups by distance from a coast.

As can be seen in Figure 29, the diurnal cycle of land divided by distance from a coast is much noisier than the entire land data because there are a third as many observations being examined. Potentially, a more cohesive and stronger diurnal cycle signal appears in the plot the further from the coast. For land less than 38km from a coast, there does

not appear to be any diurnal signal. The noise varies the same amount across the entire day. For land between 38 and 128km from a coast, there is a slight signal. For land more than 128km from a coast, there is a distinct if still slightly noisy signal. The precipitable water vapor drops off in late morning and increases for the rest of the afternoon. This difference still only accounts for an 8% change in the precipitable water vapor over the course of a day.

#### 4.4.2 PRECIPITATION

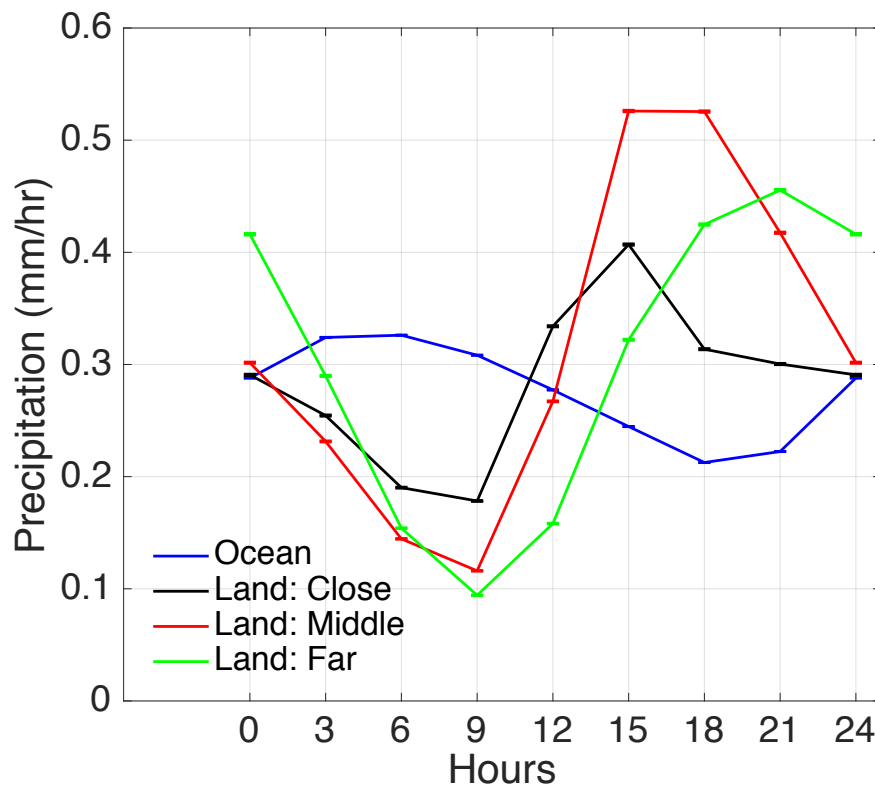


**Figure 30 | Diurnal Cycle of TRMM Observations Divided by Distance From a Coast.** The measurement at hour 24 is the same as hour 0 to allow for a complete cycle to be plotted.

The diurnal cycle of precipitation over land changes significantly when divided by distance from a coast. The most severe diurnal cycle can be seen over land that is between 38 and 128km from a coast. The

smallest diurnal cycle can be seen in land closest to the coast. There is a phase shift associated with moving inland from the coast. While the land closest from the coast is still significantly out of phase with the ocean, it is closer than the other two areas of land. While the peaks of precipitation appear to have a phase shift, the lowest levels of precipitation for all three areas of land occur at the same time?: 9:00. The time of the peak for the land within 38km of a coast is at 15:00, for between 38 and 128km is between 15:00 and 18:00, and for the land farther than 128km is at 21:00.

#### 4.5 RELATIONSHIP BETWEEN PRECIPITATION AND PRECIPITABLE WATER VAPOR BY DISTANCE FROM A COAST

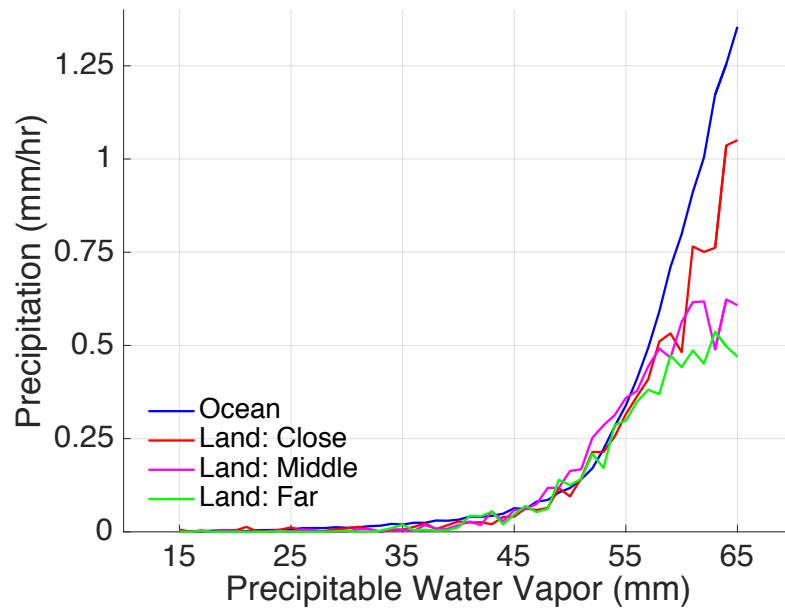


**Figure 31|Daily Mean Precipitation and Precipitable Water Vapor by Distance from a Coast.** Land close to a coast (within 38km), a middle distance from a coast (between 38 and 128km), and a far distance from a coast (more than 128km).

Distance from a coast has a large impact on the relationship between precipitation and precipitable water vapor. While much noisier than Figure 18c with all of the land combined, Figure 31 plotting the

different distances from the coast shows quite clearly the progression of the relationship between precipitation and precipitable water vapor away from the coast. As land is farther from coast, the average daily precipitation for a single given precipitable water vapor observation reaches more of a plateau. As measurements of high precipitable water were taken farther from the coast, the resulting amount of precipitation is less than it would be closer to the coast. For data taken more than 128km from a coast, there seems to be a leveling off of precipitation at 0.5mm/hr. The difference in the COSMIC and SUOMINET curves appears to be explained by this progression away from the coast. While the COSMIC data covered the entirety of the island land mass in the Maritime Continent, the SUOMINET stations were all located near a coast. The relationship between precipitation and precipitable water vapor at the locations of the SUOMINET stations would look very similar to that of the ocean.

## 4.6 STATISTICAL BOUNDS

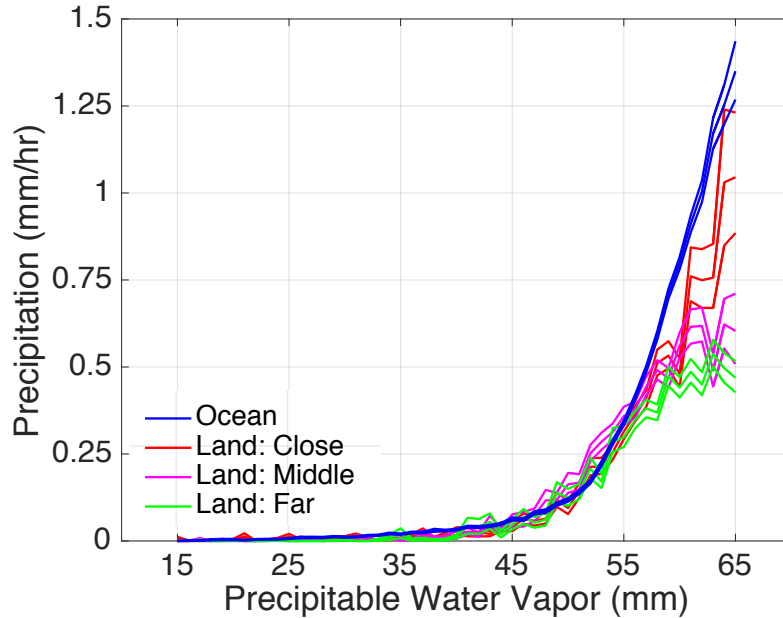


**Figure 32|Bootstrapped Distance from a Coast.** 20% replacement of 1000 runs of the mean daily TRMM precipitation and COSMIC precipitable water vapor divided by distance from a coast. The top line for each is the 95%, the middle is 50%, and the bottom is 5%.

As can be seen in Figure 32, the 95% confidence margins of the plot dividing land into thirds by distance from a coast are much larger than for the land when it is all together. Because of the smaller number of data points included into each plot, it is to be expected that the bounds would be larger. While it cannot be said that every relationship line has a 95% confidence that it is different from every other relationship, it can be said for the relationships not right next to each other. For the land more than 128km from a coast, there is more than 95% confidence that its relationship between precipitation and precipitable water vapor is different from the land closer than 38km from a coast.

## Chapter 5: Averaging COSMIC Data

All of the previous COSMIC analysis in this thesis used a single, instantaneous measurement of precipitable water vapor. There are several reasons why an averaged value of precipitable water vapor might be more accurate. It provides a more representative sampling of data in an area. It would allow for better comparison of findings to other papers such as Bretherton et al where they used multiple measurements a day. I wanted to see whether by cum

In an effort to analyze an averaged version of the data to see, I divided all the data into 1 degree by 1 degree by five-day squares. I then took only the average of blocks that had three or more water vapor measurements within. This led to very few data points—only 328 ocean data points and 95 land data points for the 10 years of data. This leads me to believe the main analysis done using an instantaneous measurement is the only one available when examining the Maritime Continent or an area of that size for the number of years that the COSMIC and TRMM projects overlap.

While averaging the COSMIC data points might have provided a more robust finding, the errors incurred from using an instantaneous measurement of water vapor to represent the entire day are low and less than they would be for using an instantaneous precipitation measurement. This can be seen from the diurnal cycles of precipitable water vapor for both the COSMIC data and the SUOMINET data. For the COSMIC precipitable water vapor diurnal cycle for the ocean and for the aggregate of land, the change across a day is roughly 2%. The diurnal cycle is potentially slightly stronger over land more than 128km from a coast but the change over the course of a day appears to be only 8%. For the SUOMINET diurnal cycles at the various stations, the change in measurement across a day is in the same magnitude.

## Chapter 6: Conclusion

### 6.1 OVERVIEW OF FINDINGS

The relationship between precipitation and precipitable water vapor over ocean and land are significantly and statistically different from each other. As land is further from a coast, the amount the relationship differs from that of the ocean increases. For land further than 128km from a coast, there appears to be a cut off for daily averaged precipitation at 0.5mm/hr. On average, no matter how much more precipitable water vapor there is, it will not rain more than 0.5mm/hr over the course of the day.

While the diurnal cycle of precipitable water is not strong for either land or ocean, there is some evidence that it becomes stronger for land further from a coast. With the amount of data from an overlap between COSMIC and TRMM, it is difficult to tell how robust this finding is because of the excess noise in the plot. The diurnal cycle of precipitation for ocean and land look fairly different from each other. Over land, the precipitation diurnal cycle is much stronger and out of phase with the diurnal cycle over the ocean. When dividing the land by distance from a coast, the precipitation diurnal cycle appears to have a phase lag moving inland. The strongest diurnal cycle is over land that is between 38 and 128km from a coast.

The changes in the the relationship of precipitation and precipitable water vapor over land with changes in temporal resolution indicate strong diurnal forcing. Over the course of a day, even with high precipitable water vapor values, the average precipitation will be less than half that over the ocean with the same amount of precipitable water vapor. This forcing may be cause the weakening in the MJO that is observed by providing high frequency convective overturning that competes with the MJO's low frequency progression.

## 6.2 FURTURE WORK

Further work needs to be done to better understand the relationship between precipitation and precipitable water vapor. As more RO projects collect data, a larger and more robust data set of precipitable water vapor observations will become available allowing for a more resolved and better constrained view of both the relationship as well the diurnal cycle. Especially for future examinations into the effect distance from a coast has on the relationship, more data points will be needed. Further work also needs to be done to verify the findings in this study. While an explanation for the disparity between the findings of SUOMINET and COSMIC was found, another precipitable water vapor data set is needed to positively corroborate the findings in this study.

The cause of the dependence on distance from a coast for the relationship between precipitation and precipitable water vapor should also be further investigated. There are many possible causes including moisture brought in from sea breezes and topography.

Much more work is needed to understand the weakening of the MJO as it passes over the Maritime Continent. This study provided some evidence for a strong diurnal effect over the islands in the Maritime Continent that may lead to the weakening but much more research needs to be done to conclude on a cause.

## References

- Anthes, R. A., Bernhardt, P. A., Chen, Y., Cucurull, L., Dymond, K. F., Ector, D., ... Zeng, Z. (2008). The COSMIC/FORMOSAT-3 mission: Early results. *American Meteorological Society*, 89 (3), 313-333. doi: 10.1175/BAMS-89-3-313.
- Bretherton, C. S., Peters, M. E., & Back, L. E. (2004). Relationships between water vapor path and precipitation over the tropical oceans. *Journal of Climate*, 17, 1517-1528. doi: 10.1175/1520-0442(2004)017(1517:RBWVPA)2.0.CO;2.
- Jacob, Daniel. *Introduction to Atmospheric Chemistry*. Princeton: Princeton University Press, 1999. *Atmospheric Chemistry Modeling Group, Harvard School of Engineering and Applied Sciences*. Web. 19 Mar. 2016.
- Kuo, Y.-H., Wee, T.-K., Sokolovskiy, S., Rocken, C., Schreiner, W., Hunt, D., & Anthes, R. A. (2004). Inversion and error estimation of GPS radio occultation data. *Journal of the Meteorological Society of Japan*, 82 (1B), 507-531. doi: 10.2151/jmsj.2004.507.
- Maloney, Eric D., & Sobel, A. H. (2004). Surface fluxes and ocean coupling in the tropical intraseasonal oscillation. *Journal of Climate*, 17 (22), 4368-4386. doi: 10.1175/JCLI-3212.1.
- Randall, David. *An Introduction to the Global Circulation of the Atmosphere*. Princeton: Princeton University Press, 2015.
- Salby, Murry L., & Hendon, Harry H. (1994). Intraseasonal behavior of clouds, temperature, and motion in the tropics. *Journal of the Atmospheric Sciences*, 51 (15), 2207-2224. [http://dx.doi.org.ezp-prod1.hul.harvard.edu/10.1175/1520-0469\(1994\)051%3C3365:C%3E2.0.CO;2](http://dx.doi.org.ezp-prod1.hul.harvard.edu/10.1175/1520-0469(1994)051%3C3365:C%3E2.0.CO;2).
- Sobel, A. H., Burleyson, C. D., & S. E. Yuter (2011). Rain on small tropical islands. *Journal of Geophysical Research*, 116.

- http://dx.doi.org.ezp-prod1.hul.harvard.edu/10.1029/2010JD014695
- Sobel, A. H., Maloney, Eric D., Bellon, Gilles, & Frierson, Dargan M. (2008). The role of surface heat fluxes in tropical intraseasonal oscillations. *Nature Geoscience*, 1 (10), 653-656. doi: 10.1038/ngeo312.
- Wang, Bin, & Li, Tianming (1993). Convective interaction with boundary-layer dynamics in the development of a tropical intraseasonal system. *Journal of the Atmospheric Sciences*, 51 (11), 1386-1400. http://dx.doi.org.ezp-prod1.hul.harvard.edu/10.1175/1520-0469(1994)051%3C1386:CIWB%3E2.0.CO;2.
- Ware, R., Exner, M., Feng, D., Gorbunov, M., Hardy, K., Herman, B., ... Trenberth, K. (1996). GPS sounding of the atmosphere from low earth orbit: Preliminary results. *Bulletin of the American Meteorological Society*, 77 (1), 19-40. http://dx.doi.org.ezp-prod1.hul.harvard.edu/10.1175/1520-0477(1996)077%3C0019:GSOTAF%3E2.0.CO;2.
- Yunck, T. P., Liu, Chao-Han, & Ware, Randolph. A history of GPS sounding. *Terrestrial, Atmospheric and Oceanic Science*, 11 (1), 1-20.
- Zhang, Chidong (2005). Madden-Julian Oscillation. *Reviews of Geophysics*, 43. doi: 10.1029/2004RG000158.
- Zhang, Chidong, & Hendon, Harry H. (1996). Propagating and standing components of the intraseasonal oscillation in tropical convection. *Journal of the Atmospheric Sciences*, 54, 741-752. doi: 10.1175/1520-0469(1997)0542.0.CO;2.